THESIS FOR THE DEGREE OF LICENTIATE OF ENGINEERING

Development of Speed-power Performance Models for Ship Voyage Optimization

XIAO LANG

Department of Mechanics and Maritime Sciences
CHALMERS UNIVERSITY OF TECHNOLOGY
Gothenburg, Sweden, 2021

Development of Speed-power Performance Models for Ship Voyage Optimization

XIAO LANG

Report No 2021:04

Chalmers University of Technology
Department of Mechanics and Maritime Sciences
Division of Marine Technology
SE-412 96, Gothenburg
Sweden
Telephone: +46 (0)31-772 1000
www.chalmers.se

Printed by Chalmers Reproservice
Gothenburg, Sweden, 2021

To my parents

Development of Speed-power Performance Models for Ship Voyage Optimization

XIAO LANG
Chalmers University of Technology
Department of Mechanics and Maritime Sciences
Division of Marine Technology

Abstract

Various measures, such as voyage optimization, performance monitoring and ship cleaning schedules, have been developed to help increase the energy efficiency of shipping operations. One of the most important elements needed for these measures is a reliable ship speed-power model. Many research efforts have been devoted to developing such models to describe a ship's energy performance for head-to-beam seas, which are important for ship design purposes. For measures to increase the energy efficiency of a ship's operations, speed-power performance models for other heading angles are of equal importance but are rarely investigated. Therefore, the overall objective of this thesis is to develop speed-power models for arbitrary wave headings that are especially applicable for ship voyage optimization. First, a semi-empirical model is proposed based on experimental tests. Then, a machine learning model (black box) is developed based on a large amount of full-scale measurement data.

For the semi-empirical model, formulas to estimate a ship's added resistance in head waves are developed to effectively describe a ship's hull forms and other main characteristics. The formulas are then extended to estimate the impacts of wave headings from different angles, and these are verified by experimental model tests. A significant wave height-based correction factor is proposed to consider the nonlinear effect on a ship's resistance and power increase due to irregular waves. For the machine learning-based model, the XGBoost algorithm is used to establish the model based on full-scale measurements of a PCTC . The input features include parameters related to ship operation profiles, metocean conditions, and motion responses.

For the three case study ships, the discrepancy between power predictions and the actual values is reduced from more than 40% using today's well-recognized methods to approximately 5% using the semi-empirical model proposed in this thesis. The machine learning model can further reduce the discrepancy to less than 1%. It is also demonstrated that the improved models can help to effectively optimize a ship's voyage planning to reduce fuel consumption.

Keywords: added resistance due to waves, energy efficiency, full-scale measurements, machine learning, speed-power performance, voyage optimization

Preface

This thesis presents research performed at the Division of Marine Technology, Department of Mechanics and Marine Sciences at Chalmers University of Technology from October 2018 to December 2020. Financial support for this research was provided by the EcoSail project (Eco-friendly and customer-driven Sail plan optimization service) and funded by the European Commission under grant agreement 820593.

As my PhD voyage is now half-way through, I would like to take the opportunity to recognize the people without whom this thesis would not have been possible.

First and foremost, I would like to express my deepest gratitude to Professor Wengang Mao for being my supervisor and for giving me the opportunity to become a PhD student. Thank you for all the guidance, nice discussions and the constant support throughout my studies, work and life that you have provided me for the last couple of years.

This gratitude also goes to my examiner and co-supervisor, Professor Jonas W, Ringsberg, head of the Division of Marine Technology. Thank you for your great support during the early stages of my academic life. Your tireless work ensures a stimulating and joyful research atmosphere in our division and brings us all forward. I offer special thanks to my co-supervisor, Associate Professor Leif Eriksson, for providing fruitful comments and guidance.

I would also like to thank the current and former members at the Division of Marine Technology. Many thanks are given to Dr. Helong Wang for all the support and encouragement you have given to me since I joined our group. Additionally, many thanks go to Dr. Da Wu for fruitful feedback and ideas. Thank you to Daiyong for the good cooperation and teamwork. I am also grateful to Dr. Shun-Han Yang and Adjunct Professor Erland Johnson for all the nice discussions and collaborations we have had. Thank you Artjoms for being a good friend and nice neighbor in the office.

Special thanks are offered to Muye, Xin and their families for all the great moments we have experienced together in Gothenburg. I would also like to thank Hao, Yigeng, and Mengcheng for always being there for me.

Finally, special thanks to my girlfriend Mengqiao for your love and tireless encouragement. I would like to express my sincerest gratitude to my dear parents for your constant support, love, and encouragement over the years.

Xiao Lang
Gothenburg, December 2020

Contents

Abstract i

Acknowledgements iii

List of appended papers vii

List of other published papers by the author ix

Nomenclature xi

1 Introduction 1
- 1.1 Background . . . 1
- 1.2 Literature review . . . 3
- 1.3 Motivation and objectives . . . 6
- 1.4 Assumptions and limitations . . . 7
- 1.5 Outline of the thesis . . . 8

2 Method for the ship speed-power modelling 9
- 2.1 General concept of ship propulsion . . . 9
- 2.2 Ship's total resistance in a real seaway . . . 10
  - 2.2.1 Calm water resistance . . . 10
  - 2.2.2 Added resistance due to wind . . . 11
  - 2.2.3 Added resistance due to waves . . . 11
- 2.3 Semi-empirical model for added resistance in waves . . . 12
  - 2.3.1 Added resistance due to wave reflection . . . 12
  - 2.3.2 Added resistance due to ship motion . . . 14
  - 2.3.3 A correction factor for ship resistance and power . . . 16

2.4 Machine learning approach 17

3 Experimental tests and full-scale measurements 23
3.1 Experimental tests on regular waves 23
3.2 Full-scale measurements from three ships 24
3.3 Metocean data 26
3.4 Data processing 26
3.4.1 Semi-empirical model 26
3.4.2 Machine learning model 28

4 Results 31
4.1 Summary of Paper I 31
4.2 Summary of Paper II 35
4.3 Summary of Paper III 38

5 Conclusions 43

6 Future work 47

References 49

List of appended papers

For each of the three appended papers, the author of this thesis contributed to the ideas presented, planned the paper with the co-authors, did the data processing, formal analysis, results visualization, and wrote the manuscript. The final review and edit are finished together with the co-authors.

Paper I **X. Lang**, W. Mao. "A semi-empirical model for ship speed loss prediction at head sea and its validation by full-scale measurements". *Ocean Engineering*, vol. 209, 107494, Aug. 2020. DOI: 10.1016/j.oceaneng.2020.107494.

Paper II **X. Lang**, W. Mao. "A practical speed loss prediction model at arbitrary wave heading for ship voyage optimization". Submitted to *Journal of Marine Science and Application* (under review), Dec. 2020.

Paper III **X. Lang**, D. Wu, W. Mao. "XGBoost method to model a ship's propulsion power in seaways". To be submitted to *Journal of Ship Research*, Oct. 2020.

List of other published papers by the author

Paper A **X. Lang**, H. Wang, W. Mao, N. Osawa. "Impact of ship operations aided by voyage optimization on a ship's fatigue assessment". *Journal of Marine Science and Technology*, Sep. 2020. DOI: 10.1007/s00773-020-00769-8.

Paper B H. Wang, **X. Lang**, W. Mao, D. Zhang, G. Storhaug. "Effectiveness of 2D optimization algorithms considering voluntary speed reduction under uncertain metocean conditions". *Ocean Engineering*, vol. 200, 107063, Mar. 2020. DOI: 10.1016/j.oceaneng.2020.107063.

Paper C J.W. Ringsberg, S. Yang, **X. Lang**, E. Johnson, J. Kamf. "Mooring forces in a floating point-absorbing WEC system - a comparison between full-scale measurements and numerical simulations". *Ships and Offshore Structures*, Mar. 2020. DOI: 10.1080/17445302.2020.1746122.

Paper D C. Zhang, D. Zhang, M. Zhang, **X. Lang**, W. Mao. "An integrated risk assessment model for safe Arctic navigation". *Transportation Research Part A: Policy and Practice*, Nov. 2020. DOI: 10.1016/j.tra.2020.10.017.

Paper E **X. Lang**, W. Mao. "A simplified ship wave induced added resistance calculation method and full-scale measurements validation in head sea". In *Proc. The 30th International Ocean and Polar Engineering Conference*, Shanghai, China, Oct. 2020.

Paper F **X. Lang**, W. Mao, D. Zhang, L.E.B. Eriksson, L. Jonasson, C. Zhang. "Comparison between full-scale measurements and theoretical fuel consumption model in a real Arctic ship navigation". In *Proc. The 29th International Ocean and Polar Engineering Conference*, Hawaii, USA, Jun. 2019.

Paper G **X. Lang**, S. Yang, J.W. Ringsberg, E. Johnson, C.G. Soares, M. Rahm. "Comparison between full-scale measurements and numerical simulations of mooring forces in a floating point-absorbing WEC system". In *Proc. The 3rd International Conference on Renewable Energies Offshore*, Lisbon, Portugal, Oct. 2018.

Nomenclature

Greek notations

α_T	Draft coefficient [-]
$(1 + \alpha_U)$	Advance coefficient [-]
β	Encountered wave heading [deg.]
ζ_a	Regular wave amplitude [m]
η_h	Hull efficiency [-]
η_o	Open water efficiency [-]
η_r	Relative rotative efficiency [-]
η_s	Shaft efficiency [-]
θ	Wave spreading direction [deg.]
λ	Wave length [m]
ρ	Water density [kg/m^3]
ρ_A	Air density [kg/m^3]
ψ_{VR}	Relative wind direction [deg.]
ω	Angular frequency [1/s]
ω_p	Angular peak frequency [1/s]
$\overline{\omega}$	Frequency factor [-]
$\overline{\omega_\beta}$	Encountered frequency factor [-]
$C_{\overline{\omega}}(\beta)$	Encountered frequency correction factor [-]

Latin notations

A_{XV}	Transverse projected area [m^2]
a_1	Amplitude factor [-]
a_2	Speed correction factor [-]
B	Ship width [m]
B_f	Bluntness coefficient [-]
BN	Beaufort number [-]
b_1	Slope adjustment factor [-]
C_{AA}	Wind resistance coefficient [-]
C_B	Block coefficient [-]

C_{H_s}	Ship propulsion power increase factor [-]
DWT	Deadweight [tonnes]
d_1	Slope adjustment factor [-]
E	Average entrance angle [deg.]
F_n	Froude number [-]
g	Gravitational acceleration [N/kg]
H_s	Significant wave height [m]
k_e	Encountered wave number [-]
k_{yy}	Longitudinal radius of gyration [-]
k_1	Form factor [-]
L_E	Length of entrance [m]
L_{pp}	Ship length between perpendicular [m]
P_b	Shaft power [kW]
P_e	Effective power [kW]
R_A	Model-ship correction resistance [N]
R_{AA}	Added resistance due to wind [N]
R_{APP}	Resistance of appendages [N]
R_{aw}	Non-dimensional added resistance due to wave [-]
R_{AW}	Added resistance due to wave [N]
R_{awr}	Non-dimensional added resistance due to wave reflection [-]
R_{awm}	Non-dimensional added resistance due to ship motion [-]
R_B	Wave resistance of bulbous bow [N]
R_{CALM}	Calm water resistance [N]
R_F	Friction resistance [N]
R_{TOTAL}	Ship total resistance [N]
R_{TR}	Additional resistance from immerses transom [N]
R_W	Wave resistance of bare hull [N]
T_{aft}	Ship draft at stern [m]
T_{fwd}	Ship draft at stem [m]
T_p	Wave peak period [s]
V	Speed through water [m/s]
V_{OG}	Speed over ground [m/s]
V_{real}	Ship real speed in a seaway [knot]

CHAPTER 1

Introduction

1.1 Background

Fluctuating fuel costs, low freight tariffs, and highly rigorous environmental regulations for decreasing greenhouse gas (GHG) emissions are promoting innovative developments of energy efficiency measures to decarbonize maritime transport. A ship's operational life typically varies from 25 to 30 years. Increasing a ship's energy efficiency could have a crucial impact from both economic and long-term environmental perspectives (Stopford, 2009).

From the economic perspective, shipping is principally a business, and its main target is to generate profit. The bunker price has exhibited volatility in the last several decades. When it exceeds \$400/mt, fuel consumption expenses could account for 50-60% of a ship's operating costs (Wang and Teo, 2013). From the environmental perspective, shipping is the backbone of international trade in the global economy, contributing to approximately 80% of global trade by volume (UNCTAD, 2018). The GHG emissions from shipping increased from 977 million tons in 2012 to 1076 million tons in 2018 (9.6% increase), and the share of shipping emissions out of the total global anthropogenic GHG emissions increased from 2.76% in 2012 to 2.89% in 2018. It is projected that shipping-induced emissions will increase up to 90-130% by 2050 relative to the emissions in 2008 (up to 50% more than the emissions in 2018).

Fossil fuel-induced emissions from shipping have attracted great attention from both public audiences and maritime authorities. To reduce GHG emissions from shipping,

as shown in Fig. 1.1, a protocol was adopted to amend the Convention, and a new Annex VI was added to the MARPOL 73/78 convention in 1997 and entered into force in 2005 for the prevention of air pollution from ships. Furthermore, the 2011 Amendments to MARPOL Annex VI introduced mandatory measures to reduce GHG emissions. A new chapter was added to Annex VI regarding "Regulations on energy efficiency for ships". Two mandatory energy efficiency mechanisms have been entered into force to regulate the energy efficiency of shipping processes, i.e., the ship energy efficiency design index (EEDI) for new ships and the ship energy efficiency management plan (SEEMP) for all ships (enacted in 2011), both of which have been mandatory since the 1st of January 2013 (IMO, 2011). In 2018, the IMO committed to cutting total annual GHG emissions from international shipping by at least 50% by 2050 (IMO, 2020).

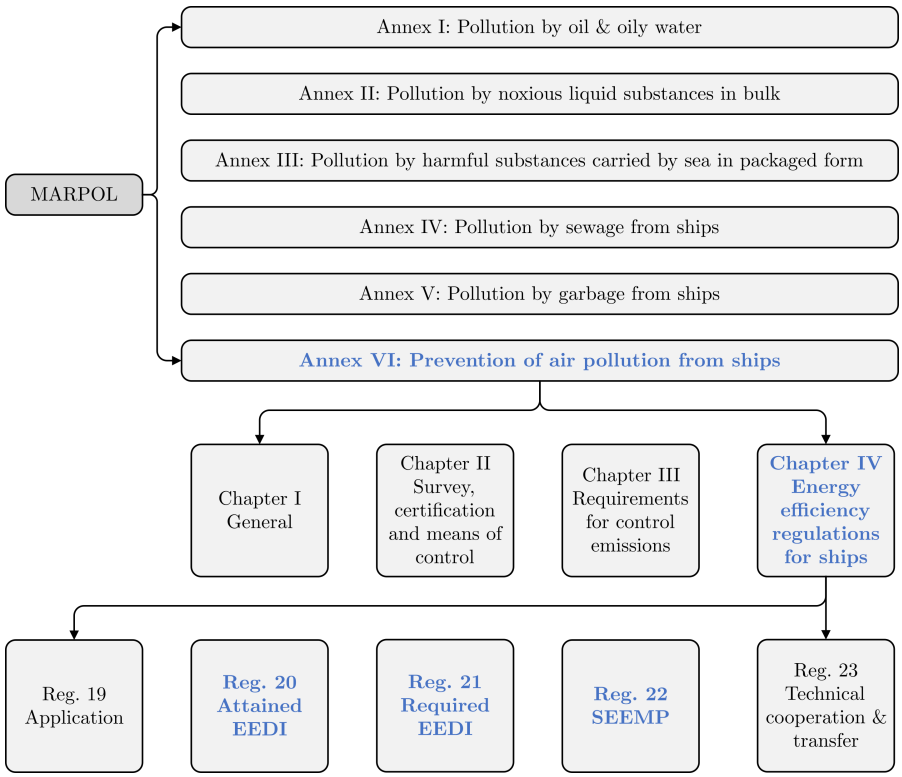

Figure 1.1: The evolution of IMO MARPOL energy efficiency regulations for ships.

All these regulations aim at reducing fuel consumption and air emissions from the shipping industry. In particular, for existing ships, the SEEMP provides a practical approach for ship operators to manage their ship operations in an energy-efficient manner over time. Various energy efficiency measures can be developed and poten-

tially installed by ships to comply with regulations such as the SEEMP. Among all the available energy efficiency measures, a ship voyage optimization system is one of the most attractive and widely implemented measures according to the shipping industry (DNV GL, 2015). With the help of voyage optimization, ships are able to avoid harsh weather conditions by choosing optimal sailing routes, leading to minimized fuel consumption (GHG emissions), reduced risk of ship/cargo damage, and increased arrival punctuality (Simonsen et al., 2015; Wang et al., 2017). During a ship's voyage optimization process, models to describe the performance of the ship at sea are the core elements for the evaluation of optimization objective functions (Wang et al., 2020; Lang et al., 2020). If a voyage optimization method is used to reduce fuel consumption, the reliability of such a method strongly depends on the accuracy of a ship's speed-power model in various ocean environments. In this thesis, various methods for establishing a ship's speed-power performance models will be investigated. The impact of using different performance models on voyage optimization will also be demonstrated. Therefore, the overall scope of the thesis is to develop reliable speed-power performance models for the development of a ship voyage optimization system.

1.2 Literature review

In a ship's energy system, some key components, such as models to estimate the ship's total resistance and propulsive coefficients, are required to describe the speed-power model. A comprehensive overview of different generic models is systematically conducted in Tillig et al. (2017). A ship's total resistance can be divided into three components, i.e., ship resistance in still water, namely, calm water resistance R_{CALM}, added resistance due to waves R_{AW} and resistance due to wind R_{AA} (Pérez Arribas, 2007). Added ice-induced resistance should also be considered if the ship sails in the Arctic region. Different model uncertainties for estimating these components and their impacts on a ship's speed-power predictions are also discussed in Tillig et al. (2018). Models used to estimate R_{CALM} and R_{AA} are often quite reliable, while for a ship's voyage optimization, it is essential to accurately estimate a ship's added resistance due to waves R_{AW}. Based on well-established seakeeping theories, models for estimating R_{AW} also include two components (Pérez Arribas, 2007). The first component is the diffraction-induced resistance when an incident wave reflects on the ship hull, dominating short waves. In the long wave region, the added resistance from waves is mainly caused by the drift force from radiated waves due to ship motions. The viscous effect is normally neglected since viscous damping is much smaller than the hydrodynamic damping of ship motions. Thus, the added resistance from waves can be regarded as a non-viscous phenomenon. This means that the added resistance obtained from model tests can be scaled up to approximate the resistance for full-scale results (Pérez Arribas, 2007). Even though experimental methods can provide

reliable results for the estimation of added resistance due to waves, the cost of doing so is often too expensive. Numerical analyses based on slender-body theory or the 3D panel method can also be used to estimate the added wave resistance (ITTC, 2018). Havelock (1942) made the first attempt to calculate such added resistance by integrating longitudinal pressure over a ship's wetted ship hull. Boese (1970) continued Havelock's work using strip theory, developing a method known as the direct pressure integration method. Maruo (1957) proposed the superposition principle, where the wave-induced added resistance is proportional to the square of the wave amplitude. The momentum conservation method was then developed according to momentum balancing through a ship hull's control volume (Maruo, 1960, 1963). The radiated energy method was initially introduced by Gerritsma and Beukelman (1972) and then further implemented in head seas for a Series 60 hull (Salvesen, 1978). In parallel to these works, Faltinsen et al. (1980) proposed asymptotic formulas to estimate added resistance for wall-side ship hulls in short waves. Often, there are large uncertainties involved in these models. For instance, accurate measurements of the reflected and diffracted resistances due to short waves are rarely obtain; these phenomena are nonlinear in nature, and the resulting values are small (Strom-Tejsen et al., 1973). Particularly, as the size of a modern ship increases, short wave regions with low λ/L_{pp} values become progressively crucial. Being able to estimate the added wave resistance correctly is hence an essential part of ship speed-power modelling .

In addition, the theoretical methods mentioned above are relatively complicated since they rely on potential flow or strip theory-based numerical analyses to estimate ship motion responses (Tillig (2020) also stated it in the ShipCLEAN model and deployed empirical methods to achieve efficient estimation). The computational effort required by such approaches typically ranges from minutes to days. Since the applications of those approaches (for the development and evaluation of energy efficient measures to guide a ship's operations, such as its voyage optimization system) generally need to run the numerical analysis procedure hundreds or thousands of times, those approaches are not feasible (ITTC, 2018).

Alternative, various semi-empirical formulas have been developed based on the aforementioned theoretical models. Fujii and Takahashi (1975) applied solutions theorized by Ursell and Dean (1947) and developed the original formula for diffraction-dominated added resistance; further development was executed by Takahashi (1988) and Tsujimoto et al. (2008) using more experimental data, resulting in the NMRI method. Simultaneously, Jinkine and Ferdinande (1974) established a semi-empirical method for quickly calculating the added resistance faced by a cargo ship in the long wave region. It was further developed for the short wave region through several joint industry projects led by MARIN; the result is known as the STAwave-1 method (Boom et al., 2013). With the support of an extracted measurement database, the

empirical STAwave-2 formula (ITTC, 2014) combines the Faltinsen et al. (1980) method for both short waves and long waves based on the technique of Jinkine and Ferdinande (1974). Recently, Liu et al. (2016) statistically simplified the combination of the above Faltinsen et al. (1980) and Jinkine and Ferdinande (1974) methods and introduced a fast approach for executing the method, denoted as NTUA in this thesis, in engineering applications according to existing experimental results. Tillig (2020) averaged STAwave-2 formula and NTUA method with an angular function for oblique waves in the ShipCLEAN model. The abovementioned wave-induced added resistance developments are briefly summarized in Figure 1.2.

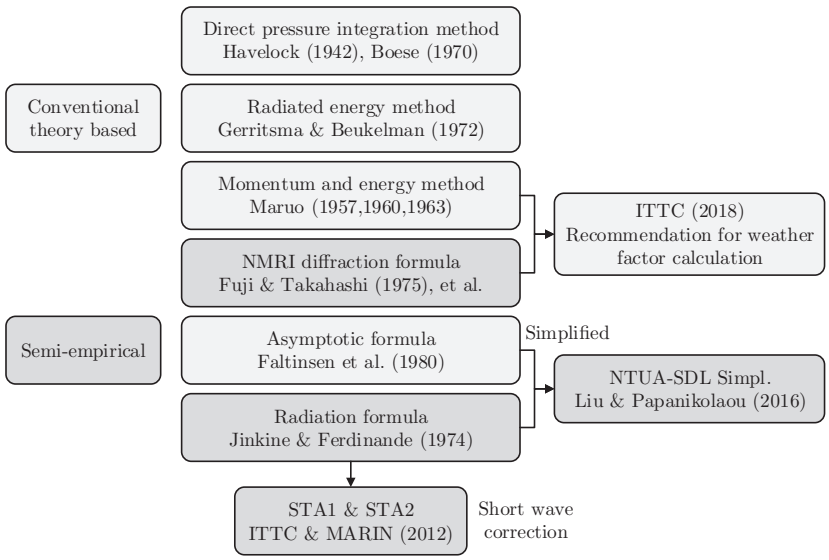

Figure 1.2: Brief summary of the development of various methods for estimating wave-induced added resistance.

Kwon (2008) extended the approximate formula developed by (Townsin and Kwon, 1982) to a direct speed loss estimation model that estimates the impact of weather in terms of the encountered wave and wind conditions. This method has been widely adopted for ship speed loss estimation in the development of voyage optimization systems (Larsson et al., 2015; Lu et al., 2015; Shao et al., 2012). In this method, only the ship type, loading condition, Froude number and block coefficient are used as inputs. Significant deviations inevitably exist between the predictive performances for specific ships. Likewise, Alexandersson (2009) proposed a simplified method to calculate added resistance through regression analysis based on a measure for a ship's motion-induced resistance that was estimated by Gerritsma and Beukelman (1972). Although this regression model is able to provide relatively acceptable estimations for long waves, it does not consider the diffraction-induced component in the short

wave region. Moreover, the accuracy decreases from the bow sea to the following sea.

With the rapid development of measurement sensor technology, today's ships are instrumented with different sensors to measure navigation-related parameters. A large amount of energy-related data is collected to effectively understand a ship's energy performance, i.e., through the ship speed-power model, while navigating at sea. Big data-driven machine learning methods have been progressively implemented for energy efficiency measures (Ballou, 2013; Mao et al., 2016a). Combinations of conventional analysis models based on physical principles and artificial neural networks (ANNs), which are called gray boxes, were first reported by Leifsson et al. (2008) and Coraddu et al. (2015) and Zhang et al. (2019). Petersen et al. (2012) compared traditional methods with a data-driven ANN method for the prediction of ship propulsion efficiency. A decision support system based on an ANN for predicting a ship's fuel consumption was proposed by Bal Beşikçi et al. (2016). Parkes et al. (2018) applied an ANN for the estimation of the shaft power of large merchant ships. Kim et al. (2020) also applied a support vector machine (SVM) to predict a vessel's propulsion power; the 2nd-order autoregressive model and other statistical mixed-effect models were also applied to establish a ship's speed-power model by Mao et al. (2016b). Uyanık et al. (2020) compared different machine learning methods for predicting the fuel consumption of a ship based on the navigational data collected while sailing.

1.3 Motivation and objectives

When navigating at sea, a ship may encounter waves from all different angles. For the development of energy efficiency measures to assist with a ship's operation, especially for voyage optimization systems, it is distinctly important to develop semi-empirical models to estimate a ship's performance while considering waves from all heading angles. However, a number of the available semi-empirical models are limited to head to beam seas, which are important for ship design purposes.

Furthermore, current semi-empirical formulas for added resistance due to waves cannot accurately estimate the resistances output by model tests, even for regular waves in head seas. For example, today's models cannot properly predict the resistance increase yielded in the short wave region when $\lambda/Lpp < 0.25$ or the resistance in a ship's motion resonance region ($\lambda/Lpp \approx 1$) (Lang and Mao, 2020). On the other hand, even though machine learning methods have been implemented by various researchers for building a ship's speed-power performance model, those machine learning models are mainly trained by general ship operation profiles, i.e., ship speed, RPM, draft, trim, etc. To apply data-driven machine learning models for energy-efficient measures, such as voyage optimization, different formulations of mathematical models used for machine learning methods should be further investigated in terms of their

power prediction capability with respect to different combinations of feature inputs, as well as their sensitivity to the volume of data used to build the models.

The main objective of this thesis is to develop ship speed-power models, particularly for the development of voyage optimization systems. Different ways to establish such performance models should be investigated, i.e., 1) physical experiment-driven semi-empirical models (white box) and 2) big data-based machine learning methods (black box). If a method is to be used for a ship's voyage optimization, the discrepancy between the measured and predicted power consumption should be less than 5-10% for the semi-empirical models (for scenarios with no measurement data available) and less than 1% for machine learning models. To achieve the overall objective, five main tasks and research activities are conducted in this thesis:

1. A semi-empirical model is developed to improve the estimation of added resistance due to regular head waves.
2. The semi-empirical model is further developed from addressing head waves to also addressing waves from arbitrary angles. These additional semi-empirical models should be developed to allow for fast calculation using as few ship characteristics as possible while achieving acceptable accuracy.
3. A data-based ship performance machine learning model is constructed to describe a ship's speed-power model and the potential increase in model accuracy over those of semi-empirical models is investigated.
4. The impact of various speed-power performance models on a ship's voyage optimization in terms of its sailing trajectories and encountered wave environments is studied.
5. The benefits of using the proposed ship speed-power performance models for voyage optimization with regard to fuel savings, emission reduction, and sailing time estimation are demonstrated.

1.4 Assumptions and limitations

A semi-empirical model requires limited input data regarding ship characteristics for power prediction. It is only verified for the design load condition. The proposed added resistance formulas cannot consider different ship drafts and trims. For the machine learning-based ship model, both stern and stem drafts are used as training features to build the performance model, which can consider draft and trim effects. However, due to the limited number of drafts collected from the full-scale measurement data, even the machine learning-based model may not be able to consider all different kinds of "unusual" drafts. For speed-power model verification or machine learning model training, several assumptions are made:

1. The full-scale measurements of ship operations and motion-related data are as-

sumed to be accurate enough to reflect a ship's actual performance when sailing in a real seaway. The sensor uncertainties that cause abnormal measurements are neglected.
2. The sea environment data from hindcast sources are assumed to be the true encountered sea environments along a ship's sailing routes because on-board measurements are not available. The historical data from the hindcast source probably offer the highest accuracy with regard to the grid points.
3. The added resistance due to waves is considered as a non-viscous phenomenon.
4. The impact of biofouling on the calm water resistance and the rudder-induced resistance are ignored.
5. The collected model test results regarding wave-induced added resistance from available publications are assumed to be correct and reliable.
6. The metocean conditions considered in this study only consist of wave, wind, and current data. The influences of the other environmental parameters, i.e., water temperature, salinity, and tide conditions, are assumed to be negligible.

Voyage optimization only considers navigation in the open sea. The objective optimization calculations, such as those for fuel consumption, are performed for the instantaneous state of a specific waypoint at a certain time. In this thesis, the instantaneous state is assumed to be a mean state during a period of stationary sea conditions. The total cost for an objective is calculated by multiplying the mean state by the time duration.

1.5 Outline of the thesis

To achieve the aforementioned objectives, the research activities carried out in this thesis are summarized in the three appended papers. A semi-empirical model for added resistance due to head waves is proposed in Paper I, and this model is extended to estimate added wave resistance for arbitrary wave headings in Paper II. The ship speed loss prediction model for actual sea states is addressed in Paper I and Paper II. Paper III investigates the efficiency and effectiveness of an XGBoost-based machine learning method for constructing a ship's speed-power model. The remainder of this thesis is organized as follows. In Chapter 2, the proposed methodology is briefly described. For the completeness of the thesis, both the general ship propulsion concept and the added resistances in the wave models developed in Papers I and II are presented, as well as the XGBoost-based machine learning algorithm investigated in Paper III. The experimental model tests for regular wave verification and the full-scale measurements for irregular wave verification and related data processing are elaborated in Chapter 3. Chapter 4 presents the selected important results and a brief summary. The conclusions are presented in Chapter 5, followed by some possible future research plans in Chapter 6.

CHAPTER 2

Method for the ship speed-power modelling

2.1 General concept of ship propulsion

A ship's energy system is a complicated process including energy consumption due to propulsion, heating, and auxiliary equipment, etc. (Woud and Stapersma, 2002). A ship's fuel consumption in a real seaway is dependent on many parameters, e.g., marine engine operating parameters, propeller efficiency, and ship resistance (Carlton, 2012). A ship's propulsion power is generally connected to the sailing speed and the encountered sea environments. For a ship's speed-power estimation, a typical workflow is illustrated in Figure 2.1.

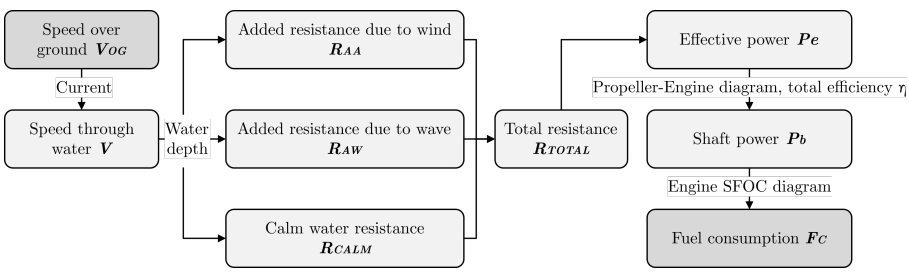

Figure 2.1: Typical workflow for the conventional estimation of a ship's speed to power/fuel consumption, and the ice induced resistance is not considered in this study.

In the workflow, the first step is to get the ship's resistance at different sailing speeds

by either model tests, numerical computation methods, or semi-empirical formulas. When a ship is sailing in a seaway, the waves and wind environments in the open sea will affect the ship's performances for most of her journey time. Hence, added resistance due to wind R_{AA} and wave R_{AW} should also be accounted for to estimate the ship's total resistance R_{TOTAL}. The ship's total resistance needs to be compensated by the thrust force provided by propellers powered by marine engines with certain RPM under different work conditions. The ship's engine configuration, propeller efficiencies, and fuel-related factors will be used to compute the propulsion power and fuel consumption for sailing under different operational and environmental conditions.

The required power to take a ship sailing forward with a ship speed through water V overcoming total resistance R_{TOTAL} is namely effective power P_e:

$$P_e = R_{TOTAL} \times V \tag{2.1}$$

where the effective power P_e is transmitted from the onboard marine engine supplied brake power P_b, that generates the shaft power to rotate the ship's propeller:

$$P_b = \frac{P_e}{\eta_s \cdot \eta_h \cdot \eta_r \cdot \eta_o} \tag{2.2}$$

where the shaft efficiency η_s, hull efficiency η_h, open water efficiency η_o, relative rotative efficiency η_r. The fuel consumption can then be predicted from the multiplication of the engine brake power P_b, with the specific fuel oil consumption (SFOC) and operation time. Dependent on the engine type and propeller properties used on a specific ship, propulsion efficiency is often provided by the manufactures, ship owners and can be used to calculate the final fuel consumption.

2.2 Ship's total resistance in a real seaway

2.2.1 Calm water resistance

An approximate calm water resistance calculation method was proposed by Holtrop and Mennen (1982), based on full-scale trails and model experiments. The method accounts for the ship main dimensions, type, appendage arrangement, immersed transom sterns. The total resistance in still water is divided into six different components:

$$R_{CALM} = R_F(1 + k_1) + R_{APP} + R_W + R_B + R_{TR} + R_A \tag{2.3}$$

where the frictional resistance R_F is estimated by ITTC-1957 frictional correlation line (ITTC, 2002), and the empirical formulas calculate the form factor $1 + k_1$, the resistance of appendages R_{APP}, wave resistance of bare hull R_W, wave resistance of bulbous bow R_B, additional resistance from immersed transom R_{TR}, model-ship

correlation resistance R_A.

Additionally, suppose the towing tank resistance test result is available. In that case, the calm water resistance is preferred to be calculated by the interpolation of the measurement value to avoid the potential deviation of different types of ships.

2.2.2 Added resistance due to wind

The wind induced added resistance is determined by the area of the ship superstructure and the relative wind. The relative wind is the vectorial summation of the ship speed, direction and wind speed, direction (Lewis, 1988). In this study, the added resistance due to wind is predicted by the ISO (2015) guideline:

$$R_{AA} = \frac{1}{2}\rho_A \left[C_{AA}\left(\psi_{WR}\right) A_{XV} {V_{WR}}^2 - C_{AA}(0) A_{XV} {V_{OG}}^2\right] \tag{2.4}$$

where the air mass density ρ_A, the transverse projected area above waterline included superstructures A_{XV}, relative wind speed V_{WR}, relative wind direction ψ_{WR}, ship speed over ground V_{OG}, the wind resistance coefficient C_{AA}, and $C_{AA}(0)$ stands for wind resistance coefficient in head wind. The wind resistance coefficients are based on the data derived from huge amount of model tests performed in the wind tunnel.

2.2.3 Added resistance due to waves

An actual sea state is usually multiplied by a spreading function $D(\theta)$ and a wave spectrum of predefined formats. In this study, a Cosine-Squared spreading function $D(\theta)$ and the the Jonswap wave spectrum, are applied to describe irregular waves of a ship's actual sailing wave conditions (Hasselmann et al., 1973):

$$D(\theta) = \begin{cases} \frac{2}{\pi} cos^2(\theta) & \text{for} -\frac{\pi}{2} \leq \theta \leq \frac{\pi}{2} \\ 0 & \text{otherwise} \end{cases} \tag{2.5}$$

$$S(\omega|H_s, T_p, \gamma) D(\theta) = \frac{320 {H_s}^2}{{T_p}^4 \omega^5} \exp\left(\frac{-1950}{{T_p}^4 \omega^4}\right) \gamma^{\exp\left[\frac{-(\omega-\omega_p)^2}{2\sigma^2 {\omega_p}^2}\right]} D(\theta) \tag{2.6}$$

where the wave spreading direction θ. The spectrum is described by the significant wave height H_s, wave peak period T_p, peakedness factor γ (set to the standard value 3.3). The spectral width parameters $\sigma = 0.07$ for $\omega \leqslant \omega_p$, $\sigma = 0.09$ when $\omega > \omega_p$.

The added resistance due to wave R_{AW} in a real seaway (irregular waves), is conventionally estimated by integrating wave resistance in regular waves $R_{aw}(\omega)$ multiplied

with the wave spectrum $S(\omega)$ over the entire range of wave frequency w:

$$R_{AW}(\omega|H_s,T_p,\gamma,V,\beta)=2\int_0^{\infty}\int_{-\frac{\pi}{2}}^{+\frac{\pi}{2}}S\left(\omega|H_s,T_p,\gamma\right)\frac{R_{aw}\left(\omega|V,\beta\right)}{\zeta_a(\omega)^2}D(\theta-\beta)d\theta d\omega \tag{2.7}$$

where $\zeta_a(\omega)$ is amplitude of the regular wave to get the added resistance $R_{aw}(\omega)$. The term R_{aw}/ζ_a^2 is often referred as the transfer function (RAOs) of a ship's added resistance in waves.

2.3 Semi-empirical model for added resistance in waves

For a ship sailing with speed V and relative wave angle β, the added resistance in regular waves of frequency ω can be evaluated by the sum of two components, i.e., added resistance due to wave reflection R_{awr}, and added resistance due to ship motions R_{awm} (Strom-Tejsen et al., 1973):

$$R_{aw}(\omega|V,\beta)=R_{awr}(\omega|V,\beta)+R_{awm}(\omega|V,\beta) \tag{2.8}$$

where $R_{awr}(\omega|V,\beta)$ and $R_{awm}(\omega|V,\beta)$ are assumed to be uncoupled. And the added resistance in waves is regarded as a non-viscous phenomenon.

2.3.1 Added resistance due to wave reflection

$R_{awr}(\omega|V,0)$ in head wave

Fujii and Takahashi (1975) introduced the semi-empirical formula for diffraction induced added resistance initially four decades ago, and it was further developed by Tsujimoto et al. (2008) as the namely NMRI method. That the added resistance due to wave reflection in head wave $R_{awr}(\omega|V,0)$ is given by $\frac{1}{2}\rho g\zeta_a^2 BB_f\alpha_T\left(1+\alpha_U\right)$, where the draft coefficient α_T and advance coefficient $(1+\alpha_U)$ have further calibrated rest on the supplementary experiment data (Kuroda et al., 2008; Takahashi, 1988; Tsujimoto et al., 2008), and the advance coefficient was determined as:

$$1+\alpha_U=1+C_UF_n,\ \text{where } C_U=\max(-310B_f+68,10) \tag{2.9}$$

where the bluntness coefficient B_f, is usually estimated by the integration method, considering the shape of water plane and encountered wave direction. The bluntness coefficient is simplified by Liu et al. (2016), it is highly correlated to the block coefficient as an approximation expression:

$$B_f=2.25\sin^2 E \tag{2.10}$$

The average entrance angle $E = \arctan(B/2L_E)$, is defined by the ship width B and length of entrance L_E. Notably, the length of entrance has been modified to the length between the fore perpendicular and the point where it reaches 99% ship width at the waterline surface (Liu et al., 2016). The latest developed draft coefficient $\alpha_T = 1 - e^{-2kT}$, was evolved instead of NMRI version of Bessel function, due to the exponential decay is observed to be more equivalent to the real physical wave energy dissipation (Liu et al., 2016; Valanto and Hong, 2015).

Whereas, it still cannot catch up the tail increase for high frequency wave reflection, for instance as DTC container, KVLCC2 tanker and HSVA cruise model tests presented in el Moctar et al. (2012), Guo and Steen (2011), Liu et al. (2016), Sadat-Hosseini et al. (2013), and Valanto and Hong (2015). In the proposed model, a wave length correction factor was thus added and tuned in NMRI expression. The new modified formula has presented much better prediction performance in the short wave region, which is matching the reasonable resistance increase owing to the extremely short wave. The formula expression is given as:

$$R_{awr}(\omega|V,0) = \frac{1}{2}\rho g \zeta_a^2 B B_f \alpha_T \left(1 + \alpha_U\right) \left(\frac{0.19}{C_B}\right)\left(\frac{\lambda}{L_{pp}}\right)^{F_n - 1.11} \tag{2.11}$$

The wave length correction factor is settled by block coefficient C_B, Froude number F_n, and the ratio between wave length λ and ship length L_{pp}. Besides, k_eT is proposed to replace kT as the non-dimensional frequency in the draft coefficient:

$$\alpha_T = 1 - e^{-2k_eT} \tag{2.12}$$

where $k_e = k(1 + \Omega\cos\beta)^2$ and $\Omega = \frac{\omega V}{g}$, the circular frequency of incident regular waves ω, wave number of incident regular waves k.

$R_{awr}(\omega|V,\beta)$ at arbitrary wave heading

For the added resistance due to wave reflection at other encountered relative wave angles, the magnitude of $R_{awr}(\omega|V,\beta)$ has has shown a decline from the head wave till the following sea, as the heading angle β increase. And minor negative values are observed in the HSVA cruise, DTC container, and a bulk carrier model tests in, e.g., el Moctar et al. (2012), Kadomatsu (1988), and Valanto and Hong (2015), for a few very short waves at $120° \leqslant \beta \leqslant 180°$. Thus, a simplified modification factor $\cos\beta$ is proposed to express the physical phenomenon.

Besides, the advance coefficient is further parameter tuned by Froude number F_n, and the encountered relative wave angle β. That the resistance force has been investigated a obvious increase when $\beta \leqslant 90°$, and the negative values becomes becomes weaker when β exceed 90°, with higher F_n (ship speed). The modified added resistance due

to wave reflection for arbitrary relative wave angles is written as:

$$R_{awr}(\omega|V,\beta) = \begin{cases} R_{awr}(\omega|V,0)\cdot F_n^{(\lfloor\cos\beta\rfloor-\lceil\cos\beta\rceil)F_n}\cos\beta & \text{for } 0 \leqslant \beta \leqslant \frac{\pi}{2} \\ R_{awr}(\omega|V,0)\cdot F_n^{-1.5(\lfloor\cos\beta\rfloor+\lceil\cos\beta\rceil)F_n}\cos\beta & \text{for } \frac{\pi}{2} < \beta \leqslant \pi \end{cases} \tag{2.13}$$

2.3.2 Added resistance due to ship motion

$R_{awm}(\omega|V,0)$ in head wave

In parallel to NMRI formula, Jinkine and Ferdinande (1974) developed their approximate formula for ship motion induced added resistance calculation in the long wave region. This formula was derived by the experiment data of a fine hull fast cargo ship for $F_n \geq 0.12$ condition. The original model is given by:

$$R_{awm}(\omega|V,0) = 4\rho g\zeta_a^2 B^2/L_{pp}\overline{\omega}^{b_1}\exp\left[\frac{b_1}{d_1}\left(1-\overline{\omega}^{d_1}\right)\right]a_1 a_2 \tag{2.14}$$

where the amplitude factor a_1, speed correction factor a_2, slope adjustment factor b_1, d_1, and frequency factor $\overline{\omega}$. The amplitude factor came up with by Jinkine and Ferdinande (1974) has been continually modified. The most recent expression was developed by Liu et al. (2016), and further parameters tuned in this study viz:

$$a_1 = 60.3{C_B}^{1.34}\left(\frac{1}{C_B}\right)^{1+F_n} \tag{2.15}$$

while block coefficient C_B and Froude number F_n were used as modification parameters. The speed correction factor a_2 has been extended to the span $0 \leqslant F_n \leqslant 0.3$, compared to the original high speed domain (Grin, 2012; ITTC, 2014; Liu et al., 2016). The speed correction factor a_2 is found sensitive to the longitudinal radius of gyration k_{yy} and the block coefficient C_B in high speed region, through the careful analysis of all collected experimental data. Moreover, it has a little bit steeper slope compared to the formula in Liu et al. (2016) when $F_n < 0.12$. Hence the following formula is consequently introduced:

$$a_2 = \begin{cases} 0.0072 + 0.24F_n & \text{for } F_n < 0.12 \\ {F_n}^{-1.05C_B+2.3}\exp((-2-\lceil\frac{k_{yy}}{0.25}\rceil-\lfloor\frac{k_{yy}}{0.25}\rfloor)F_n) & \text{for } F_n \geq 0.12 \end{cases} \tag{2.16}$$

where the ceiling function and floor function allow to give discrete scales for F_n, concerning the correlation between k_{yy} and the typical value 0.25 (ITTC, 2017).

The frequency factor $\overline{\omega}$ is determined by the frequency of heave and pitch motions. These motions' resonance responses are regarded as the leading cause of radiation induced added resistance reaching the peak value in head wave. Liu et al. (2016) have separated the expression to lower and normal speed. However, it can still not match the experimental data well for some cases when k_{yy} do not equal to 0.25, especially for HSVA cruise (Liu et al., 2016; Valanto and Hong, 2015). The resonance position has been observed that moves horizontally from $\lambda/L_{pp} < 1$ to $\lambda/L_{pp} > 1$ region with higher Froude number F_n. The longitudinal radius of gyration variation also influences the trend. Consequently, the expression is further parameter tuned in this study, and the modified formula is given by:

$$\overline{\omega} = \begin{cases} \dfrac{\sqrt{L_{pp}/g}\ \sqrt[c_1]{\frac{k_{yy}}{L_{pp}}}0.05^{0.143}}{1.09 + \lceil \frac{k_{yy}}{0.25} \rceil 0.08}\omega & \text{for } F_n < 0.05 \\ \dfrac{\sqrt{L_{pp}/g}\ \sqrt[c_1]{\frac{k_{yy}}{L_{pp}}}F_n{}^{0.143}}{1.09 + \lceil \frac{k_{yy}}{0.25} \rceil 0.08}\omega & \text{for } F_n \geq 0.05 \end{cases} \tag{2.17}$$

where the root $c_1 = 0.4567\frac{C_B}{k_{yy}} + 1.689$, and the improved expression results are more fit to the resonance position in experiment measurements. The slope adjustment factors are also further calibrated in this study, concerning the longitudinal radius of gyration k_{yy} and the block coefficient C_B:

$$b_1 = \begin{cases} (19.77\frac{C_B}{k_{yy}} - 36.39)/\lceil \frac{k_{yy}}{0.25} \rceil & \text{for } \overline{\omega} < 1, C_B < 0.75 \\ 11/\lceil \frac{k_{yy}}{0.25} \rceil & \text{for } \overline{\omega} < 1, C_B \geqslant 0.75 \\ -12.5/\lceil \frac{k_{yy}}{0.25} \rceil & \text{for } \overline{\omega} \geqslant 1, C_B < 0.75 \\ -5.5/\lceil \frac{k_{yy}}{0.25} \rceil & \text{for } \overline{\omega} \geqslant 1, C_B \geqslant 0.75 \end{cases} \tag{2.18}$$

$$d_1 = \begin{cases} 14 & \text{for } \overline{\omega} < 1, C_B < 0.75 \\ 566\left(\frac{L_{pp}}{B}\right)^{-2.66} \cdot 2 & \text{for } \overline{\omega} < 1, C_B \geqslant 0.75 \\ -566\left(\frac{L_{pp}}{B}\right)^{-2.66} \cdot 6 & \text{elsewhere} \end{cases} \tag{2.19}$$

while $C_B = 0.75$ is adopted as the boundary to define the piece-wise.

$R_{awm}(\omega|V,\beta)$ at arbitrary wave heading

In view of the ship motions induced added resistance $R_{awm}(\omega|V,\beta)$ at arbitrary wave heading, it is still mainly caused by the long waves (small values of ω) attacking from various angles, and reaching peak value at ship motion's resonance state. From the

collected experimental tests, e.g., el Moctar et al. (2012), Fujii and Takahashi (1975), Journée (2001), Kadomatsu (1988), Liu et al. (2016), Takahashi (1988), and Valanto and Hong (2015), its peak position moves horizontally from $\lambda/L_{pp} = 1$ position to lower λ/L_{pp} region, as the encountered wave angles β increase. It can be readily explained that the encountered frequency $\overline{\omega_\beta}$ decreases from the head wave till the following wave. Thus, a novel encountered frequency correction factor $C_{\overline{\omega}}(\beta)$ was introduced in this study:

$$\overline{\omega_\beta} = \overline{\omega} * C_{\overline{\omega}}(\beta) \tag{2.20}$$

where the suggested values of $C_{\overline{\omega}}(\beta)$ for typical wave angles are listed in Table 2.1, and $C_{\overline{\omega}}(\beta)$ value of other specific encountered wave angles can be further interpolated.

Table 2.1: Encountered frequency correction factor for typical relative wave angle

β	0°	30°	45°	60°	90°	120°	135°	150°	180°
$C_{\overline{\omega}}(\beta)$	1	0.925	0.9	0.8	0.75	0.7	0.7	0.7	0.6

Besides, the $R_{awm}(\omega|V,\beta)$ peak value shows a declining trend as the relative wave angle β increases. The roll motion dominates the ship motion instead of heave and pitch motions when β close to 90°. An amplitude adjustment factor $e^{-(\frac{\beta}{\pi})^4\sqrt{F_n}}$, and a compensation factor for roll motion, considering the ratio between wave length λ and ship width B, Froude number F_n and the relative wave angle β, are thus tuned in the proposed formula:

$$R_{awm}(\omega|V,\beta) = R_{awm} \cdot e^{-(\frac{\beta}{\pi})^4\sqrt{F_n}} + [\frac{\lambda}{B} \cdot \max(\cos\beta, 0.45)]^{-6F_n}\sin\beta \tag{2.21}$$

2.3.3 A correction factor for ship resistance and power

The conventional integration method from ITTC (2014) and ISO (2015) made significant contributions to the EEDI implementation for ship design. It considers wave effect through extensive benchmark study of experimental test results and sea trails. The semi-empirical methods developed by ITTC (2014), ISO (2015), and other scholars can give a fair estimation of the "mean" wave resistance of large ship samples for the design purpose. For a ship's operation, such as in her voyage optimization planning, the specific ship's actual performance is interested rather than the "average" wave resistance.

However, the discrepancy between the estimations from the linear superposition principle and the ship's actual wave resistance cannot be avoided for an individual ship. The integration method assumes the ship's response is linear to the wave. However, a ship's response (reflections, motions) is known to be nonlinear, especially in harsher

sea states with large H_s. The propulsion efficiency may also be reduced due to the large nonlinear motions in severe sea wave conditions. Large waves lead a ship has to experience unstable surf-riding along the waves as well. These factors contribute to the propulsion power increase. All of them are strongly related to the increase of sea states H_s that directly determine the added resistance due to waves R_{AW}. Therefore, a correction factor C_{H_s} is proposed to calibrate the semi-empirical R_{AW} to consider these factors contribution to the propulsion power increase, for voyage optimization purpose. The ship total resistance R_{TOTAL} is estimated by:

$$R_{TOTAL} = R_{CALM} + R_{AA} + R_{AW} \times C_{H_s} \tag{2.22}$$

where the correction factor is wave height based $C_{H_s} = \sqrt[3.5]{H_s}$. For this correction factor's more general application, a comprehensive investigation with extra experimental tests and full-scale measurement should be conducted to configure a flexible formula, based on various input parameters.

2.4 Machine learning approach

A novel, simple tree-based ensemble method named eXtreme Gradient Boosting (XGBoost) was recently developed by Chen and Guestrin (2016). It is an improved version of gradient boosting with higher computation efficiency and better capability to deal with over-fitting problems. Despite the widely used machine learning method in the maritime industry, such as the support vector machine (SVM), artificial neural network (ANN), the XGBoost algorithm is rarely applied in ship performance studies. The XGBoost is robust to handle heterogeneous data. Especially for the onboard data, that the features are measured on different scales.

The XGBoost method is based on gradient tree boosting algorithms (Friedman et al., 2000). Gradient boosting is one of the most powerful techniques for constructing predictive models. It is a representative algorithm for boosting in the ensemble method. The ensemble method builds multiple weak evaluators on the data. It ensembles all weak evaluators' modelling results to obtain better regression or classification performance than a single model. A weak evaluator is defined as a model that performs at least better than random guessing, that is, any model with a prediction accuracy rate of not less than 50%. There are many methods to ensemble different weak evaluators. Such as the bagging method that multiple parallel independent weak evaluators established at once in random forests. There is also a method like boosting that builds weak evaluators one by one and gradually accumulates multiple weak evaluators after multiple iterations. The most famous algorithms of the boosting method include Adaboost and the gradient tree boosting. The gradient tree boosting can have regression trees or classification trees. Both use the classification and regression trees

(CART) algorithm as the mainstream. XGBoost is also a CART, which means that all trees in XGBoost are binary.

Gradient boosting decision tree (GBDT) for regression is a boosting model focusing on the regression. The modelling process is typically building a tree first. Then each iteration process gradually adds a tree and ensemble a strong evaluator with many trees. The value on each leaf node of the GBDT is the mean value of all samples on this leaf node. The prediction result of each sample can be expressed as a weighted calculation of all trees' results. It is worth noting that XGBoost is an improvement of GBDT. For XGBoost, each leaf node has a prediction score, also known as leaf weight. The leaf weight is the regression value of all the samples on this leaf node on this tree, represented by $f_k(x_i)$ or w, where f_k represents the k-th decision tree, and x_i represents the feature corresponding to the sample. When there is only one tree, $f_1(x_i)$ is returned by the boosting algorithm, but this result is often terrible. When there are multiple trees, the ensemble model's regression result is the sum of the prediction scores of all trees. Assuming that there are a total of K decision trees in the ensemble model, the prediction result given by the model on this sample is:

$$\hat{y}_i^{(k)} = \sum_{k}^{K} f_k\left(x_i\right) \tag{2.23}$$

To solve the optimal result of the ensemble algorithm, then we should find a objective function first. The objective function should be able to measure the gradient tree boosting capacity on the sample by bringing in the prediction results. Then the gradient descent is applied to iterate the ensemble algorithm:

$$\hat{y_i}^{(k+1)} = \hat{y}_i^{(k)} + f_{k+1}\left(x_i\right) \tag{2.24}$$

where after k iterations, there are a total of k trees in the ensemble algorithm. The ensemble result of k trees is the cumulation of the leaf weights on all the previous trees. So we add the ensemble results $\hat{y}_i^{(k)}$ of k trees to the leaf weights $f_{k+1}\left(x_i\right)$ on our newly-built trees to get the prediction results $\hat{y_i}^{(k+1)}$ of a total of $k+1$ trees after the $k+1$ iteration. Let this process continue until find the $\hat{y}$ that minimizes the objective function. This is the predicted result of the model.

The XGBoost is an algorithm that achieves a balance between model performance and computing speed. Standard objective functions, such as error rate, mean square error, etc., can only measure the model's performance but cannot measure its computational efficiency. The XGBoost algorithm introduces model complexity to measure computational efficiency. Therefore, the objective function of XGBoost is written as

a traditional loss function + model complexity:

$$Obj = \sum_{i=1}^{m} l\left(y_i, \hat{y}_i\right) + \sum_{k=1}^{K} \Omega\left(f_k\right) \tag{2.25}$$

where i represents the i-th sample in the dataset, m represents the total amount of data imported into the k-th tree, and K represents all the trees built. The first term represents the traditional loss function, which measures the difference between the real value y_i and the predicted value $\hat{y}_i$, usually RMSE, the root mean square error. The second term represents the model's complexity, that measures the complexity of the tree model from the structure of the tree. Combining Equation (2.24) and Equation (2.25), the objective function of the t-th iteration is:

$$Obj^{(t)} = \sum_{i=1}^{m} l\left(y_i^t, \hat{y}_i^{(t-1)} + f_t\left(x_i\right)\right) + \sum_{k=1}^{t-1} \Omega\left(f_k\right) + \Omega\left(f_t\right) \tag{2.26}$$

where f_t is the newly added tree at the t-th iteration. Through the Taylor expansion, we can obtain a simplified version of objective function without constants:

$$\begin{aligned} Obj^{(t)} &= \sum_{i=1}^{m} \left[l\left(y_i^t, \hat{y}_i^{(t-1)}\right) + f_t\left(x_i\right) g_i + \frac{1}{2}\left(f_t\left(x_i\right)\right)^2 h_i \right] + \sum_{k=1}^{t-1} \Omega\left(f_k\right) + \Omega\left(f_t\right) \\ &= \sum_{i=1}^{m} \left[f_t\left(x_i\right) g_i + \frac{1}{2}\left(f_t\left(x_i\right)\right)^2 h_i \right] + \Omega\left(f_t\right) \end{aligned} \tag{2.27}$$

where g_i and h_i are the first and second derivative of the cost function $l(y_i^t, \hat{y}_i^{(t-1)})$ with respect to $\hat{y}_i^{(t-1)}$, respectively. In this tree structure, we use $q(x_i)$ to represent the leaf node where the sample x_i is located, and use $w_{q(x_i)}$ to represent the score obtained by the sample falling on the $q(x_i)$-th leaf node on the t-th tree, so we obtained $f_t\left(x_i\right) = w_{q(x_i)}$. This is the leaf weight for each sample, but the leaf weights corresponding to all samples on a leaf node are the same. Suppose a tree contains a total of T leaf nodes, where each leaf node's index is j, then the sample weight on this leaf node is w_j, and we define the complexity of the model $\Omega(f)$ as:

$$\Omega(f) = \gamma T + regularization \tag{2.28}$$

where the first part controls the tree structure, and the other part is the regularization term. The number of leaves T represent the entire tree structure. Since all trees in XGBoost are CART (binary trees), so we can judge the depth of the tree based on the number of leaves, and γ is the parameter to control the number of leaves. If $L2$ regularization (Ridge Regression) is applied, we further simplify the objective

function from Equation 2.27:

$$\begin{aligned} Obj^{(t)} &= \sum_{i=1}^{m} \left[w_{q(x_i)} g_i + \frac{1}{2} w_{q(x_i)}^2 h_i \right] + \gamma T + \frac{1}{2} \lambda \sum_{j=1}^{T} w_j^2 \\ &= \sum_{j=1}^{T} \left[w_j \sum_{i \in I_j} g_i + \frac{1}{2} w_j^2 (\sum_{i \in I_j} h_i + \lambda) \right] + \gamma T \end{aligned} \tag{2.29}$$

where λ is a parameter that controls the intensity of $L2$ regularization. We can also use $L1$ regularization (Lasso Regression), that the parameter is α. Alternatively, it can be used together to increase the intensity of regularization. When both α and λ are 0, the objective function is the same as ordinary gradient tree boosting.

To minimize the objective function, as long as the quadratic function under each leaf's value is the smallest, their sum will be the smallest. Therefore, we take the derivative of w_j and make the first derivative equal to 0 to find the extreme value, then obtain $w_j = -\frac{G_j}{H_i + \lambda}$, and the corresponding optimal value is:

$$Obj^{(t)} = -\frac{1}{2} \sum_{j=1}^{T} \frac{G_j^2}{H_j + \lambda} + \gamma T \tag{2.30}$$

where define $G_j = \sum_{i \in I_j} g_i, H_j = \sum_{i \in I_j} h_i$. Compared to the original loss function + complexity, the XGBoost's objective function has changed dramatically. The sample has been attributed to each leaf. The objective function is calculated based on each leaf node, which is the structure of the tree. Therefore, the objective function is also called "structure score". The score is lower as the better of the overall structure of the tree. In this way, a direct connection between the tree's structure (leaf) and the effect of the model is established. To minimize the objective function is to find the best tree's structure (T). Then the G_j, H_j and further w_j are evaluated.

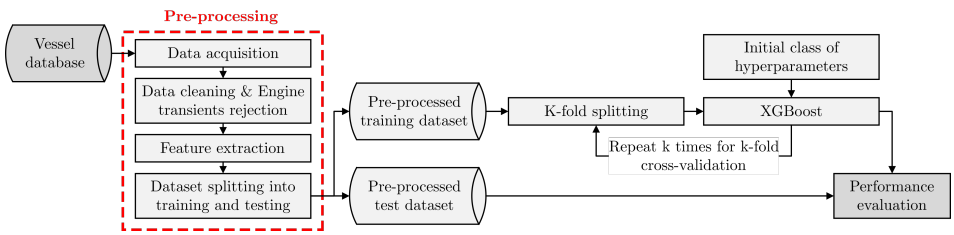

Figure 2.2: Workflow for the suggested machine learning methodology based on XGBoost algorithm.

In this thesis, the non-linear tree-based learner in XGBoost is applied for the regression task of ship speed-power modelling. The developed methodology based on

XGBoost algorithm is illustrated in Figure 2.2. The full-scale measurements of the studied PCTC is pre-processed and implemented in feature engineering. The dataset is then randomly split into training (80%) and testing (20%) set. The 5-fold cross-validation is implemented in the hyperparameters tuning process to minimize the generalization errors of model training.

Table 2.2: Attributes filtered and considered for the proposed XGBoost model

Class	Category	Description	Attributes
Input attributes	Operation	Ship speed	V [knots]
		Ship draft	T_{fwd} & T_{aft} [m]
		Heading	HDG [°]
	Ship motions	6 DOF motions	$Heave$ & $Sway$ & $Surge$ [m]
			$Roll$ & Yaw & $Pitch$ [°]
		Velocity of 6 DOF motions	$Heave_{vel}$ & $Sway_{vel}$ & $Surge_{vel}$ [m/s]
			$Roll_{vel}$ & Yaw_{vel} & $Pitch_{vel}$ [°/s]
		Acceleration of 6 DOF motions	$Heave_{acc}$ & $Sway_{acc}$ & $Surge_{acc}$ [m/s^2]
			$Roll_{acc}$ & Yaw_{acc} & $Pitch_{acc}$ [°/s^2]
	Metocean environments	Significant wave height	H_s [m]
		Mean wave period	T_z [s]
		Mean wave direction	D_{wave} [°]
		Wind speed	U_{wind} & V_{wind}
Output target	Operation	Propulsion power	P_b [kW]

To establish a ship's speed-power model, the parameters related to the prediction target of propulsion power is required to set as input features to the training dataset. For a ship voyage optimization system and knowledge gaps identified in the semi-empirical model development, the encountered metocean environments are the essential features for the model training, except for the operation profiles, such as ship speed through water V, ship draft at stem T_{fwd} and stern T_{aft}. During a ship in a real seaway, the encountered wave and wind always induce 6 DOF motion responses of ship. Thus, it is also interested to deploy the ship's motions as input features instead of metocean loads with a more straightforward way. The details of the considered features for the modelling is summarized in Table 2.2. The ship operation and metocean environments dataset are applied for metocean based machine learning model. The motion driven model consist of ship operation and motion dataset. At the same time, the 1st and 2nd derivative of the 6 DOF is studied separately.

CHAPTER 3

Experimental tests and full-scale measurements

In this thesis, the proposed semi-empirical models are verified with both experimental test data and full-scale measurement data. The machine learning models are derived from full-scale measurements of a PCTC ship. In the following sections, various types of data are briefly presented. Since the full-scale measurement data often contain some measurement noise, the data postprocessing approaches used in the thesis to clean the data and obtain a reliable reference for model verification are presented.

3.1 Experimental tests on regular waves

The proposed semi-empirical formulas for estimating a ship's added resistance due to waves, as presented in Section 2, are developed based on experimental tests on regular waves. Several model tests are available in the public literature and are collected for this study, i.e., S175 container (Fujii and Takahashi, 1975; Takahashi, 1988), KVLCC2 tanker (Guo and Steen, 2011; Sadat-Hosseini et al., 2013), DTC container (el Moctar et al., 2012), HSVA cruise (Valanto and Hong, 2015), S.A. Van Der Stel (Alexandersson, 2009), a bulk carrier (Kadomatsu, 1988), and Series 60 models with five various block coefficients C_B (Strom-Tejsen et al., 1973). All the required parameters for those ships are listed in Table 3.1. For the development and verification of the semi-empirical models on regular head waves, the experimental results from all 11 aforementioned ships are employed in Paper I. Five ships, i.e., the S175 container ship, the DTC container ship, the HSVA cruise ship, the S.A. Van Der Stel and the bulk carrier, are selected to verify the semi-empirical model

for added resistance due to arbitrary wave heading angles. Table 3.2 presents the considered relative wave angles β and Froude numbers F_n of the experimental tests in Paper II.

Table 3.1: Main characteristics of the studied ships in the experiments conducted in available publications.

Ship type	L_{pp} [m]	B [m]	T [m]	C_B [-]	L_E [m]	k_{yy} [-]
S175 container	175	25.4	9.5	0.572	59.05	0.24
KVLCC2 tanker	320	58	20.8	0.8098	60	0.25
DTC container	355	51	14.5	0.661	112	0.27
HSVA cruise	220.27	32.2	7.2	0.654	72.42	0.263
S.A. Van Der Stel	152.5	22.8	9.14	0.563	61	0.22
Bulk carrier	285	50	18.5	0.829	51	0.25
Series 60 model 4210	121.96	16.254	6.492	0.6	52	0.25
Series 60 model 4211	121.96	16.816	6.73	0.65	46.522	0.25
Series 60 model 4212	121.96	17.42	6.97	0.7	38.606	0.25
Series 60 model 4213	121.96	18.062	7.22	0.75	30.48	0.25
Series 60 model 4214	121.96	18.757	7.495	0.8	22.8	0.25

Table 3.2: Considered relative wave angles and Froude numbers for arbitrary wave heading model tests.

Ship type	Relative wave angle β	Froude number F_n
S175 container	[0°, 30°, 60°, 90°, 120°, 150°, 180°]	0.250
DTC container	[0°, 30°, 60°, 120°, 150°, 180°]	0.052
HSVA cruise	[0°, 30°, 60°, 90°, 120°, 150°, 180°]	0.232
S.A. Van Der Stel	180°	[0.150, 0.200, 0.250, 0.300]
Bulk carrier	[0°, 45°, 90°, 135°, 180°]	0.100

3.2 Full-scale measurements from three ships

A merchant chemical tanker and a PCTC sailing worldwide, as well as a container ship sailing in the North Atlantic, are employed as the case study vessels. The full-scale measurement data collected onboard these vessels are used to verify the proposed semi-empirical models. The main characteristics of these studied ships are listed in Table 3.3. These parameters are applied as inputs in the semi-empirical models. The three ships were instrumented with various sensors to collect a large amount of ship navigation- and performance-related data, up to a gigabyte per day. The parameters of the full-scale measurement data from all three ships are similar.

Table 3.3: Main characteristics of the studied PCTC, container ship and chemical tanker used for full-scale measurements.

Parameter	Symbol	Unit	PCTC	Container	Chemical tanker
Length between perpendicular	L_{pp}	m	190	232	174.8
Breadth molded	B	m	32.26	32.2	32.2
Designed draft	T	m	9.5	10.78	10.98
Block coefficient	C_B	-	0.6	0.54	0.8005
Longitudinal radius of gyration	k_{yy}	-	0.26	0.26	0.25
Length of entrance	L_E	m	62	40	38.5
Transverse projected area	A_{XV}	m^2	985	750	400
Deadweight	DWT	tons	28126	40900	46067
Maximum continuous rating	P_c	kW	14700	21000	8200

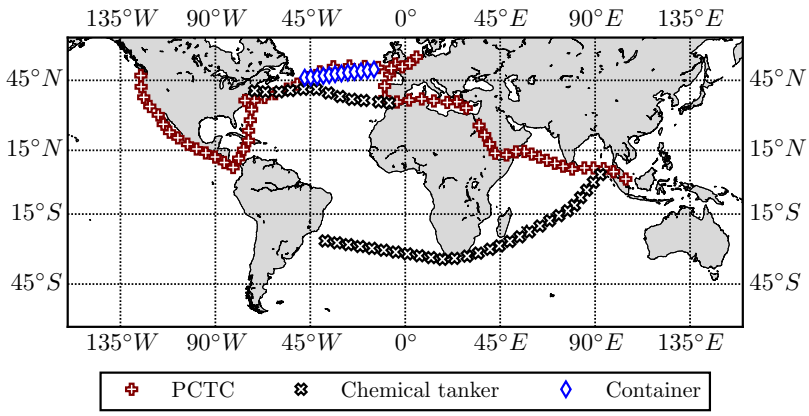

Figure 3.1: Typical routes of the three studied ships during their measurement campaigns. The PCTC and chemical tanker were sailing worldwide, while the container ship was sailing in the North Atlantic.

In the full-scale measurements, the shaft torque, RPM and propulsive power were recorded by sensors installed in marine engines. The ship draft was measured at the stern and stem. A GPS tracker stored the longitude, latitude, speed over ground, and ship heading at the wheelhouse of each ship. The measurements were collected with a frequency of 1 Hz. Several typical sailing routes recorded during the full-scale measurement campaign are illustrated in Figure 3.1. Furthermore, the ship baselines used to describe the calm water resistances obtained from model tests and sea trials are provided by the ship operators for this study. The coefficient of wind resistance for the PCTC is obtained from wind tunnel tests. For the chemical tanker and the container ship, the wind resistance R_{AA} is calculated according to the semi-empirical

models in ISO (2015). The total propulsive efficiency η_D is extracted from the open water tests.

3.3 Metocean data

For the development of a ship's speed-power model and the investigation of its impact on voyage optimization, it is crucial to access reliable meteorological and oceanographic (metocean) environments that are encountered by ships. A metocean environment includes parameters for wind, waves and currents. For the purposes of both the development and verification of a ship's speed-power performance in terms of its encountered metocean environment, actual historical data from different hindcast data sources are used. In this study, the mean wave direction D_{wave}, mean wave period T_z, significant wave height H_s, and wind speed U_{wind} and V_{wind} are extracted from the reanalysis dataset ERA5 to construct the encountered sea states along the sailing routes (Copernicus, 2019). In terms of the current speed $U_{current}$ and $V_{current}$, the CMEMS (2019) observation data are applied. The U component denotes the speed from west to east, and the V component denotes the speed from south to north for both wind and currents. The true velocity and direction are the vectorial summation of these two components. The spatial and temporal resolutions of the metocean parameters used in this study are listed in Table 3.4. The bathymetry information is accessed from GEBCO (2019). The environmental loads caused by biofouling are ignored in this study.

Table 3.4: Sources and resolutions of the metocean parameters used in this study.

Parameter	Source	Spatial resolution	Temporal resolution
H_s T_z D_{wave} U_{wind} V_{wind}	ERA5	0.25×0.25 degree	hourly
$U_{current}$ $V_{current}$	CMEMS	0.25×0.25 degree	daily

3.4 Data processing

3.4.1 Semi-empirical model

Full-scale measurement data are used to verify the semi-empirical speed-power model for speed loss prediction. To predict a ship's speed loss, the power setting should

be first identified from the full-scale measurements. In this study, all the sailing waypoints from engine power settings close to 9000 kW (64% MCR) for the PCTC, 17000 kW (80% MCR) for the container and 5800 kW (70% MCR) for the chemical tanker are selected for the verification analysis.

The Kwon (2008) model that is widely used in ship voyage optimization systems is compared with the semi-empirical speed-power models developed in this study. It takes Beaufort numbers as inputs to predict a ship's speed loss. Therefore, for the full-scale measurements of the three case study ships, all the waypoints from the selected engine power settings are divided into various Beaufort number groups, i.e., BN-3, BN-4, BN-5, BN-6, and BN-7, based on the encountered significant wave height H_s. The interval of H_s for determining the Beaufort numbers of encountered metocean environments is determined according to Table 3.5, which uses criteria from the definitions in ISO (2015).

Table 3.5: The probable span of H_s for the Beaufort scales considered in the verification dataset separation process.

Beaufort number	Significant wave height	Beaufort number	Significant wave height
BN-3	$0.3 \sim 1.0$ m	BN-4	$1.0 \sim 1.5$ m
BN-5	$1.5 \sim 2.5$ m	BN-6	$2.5 \sim 4.0$ m
BN-7	$4.0 \sim 5.5$ m		

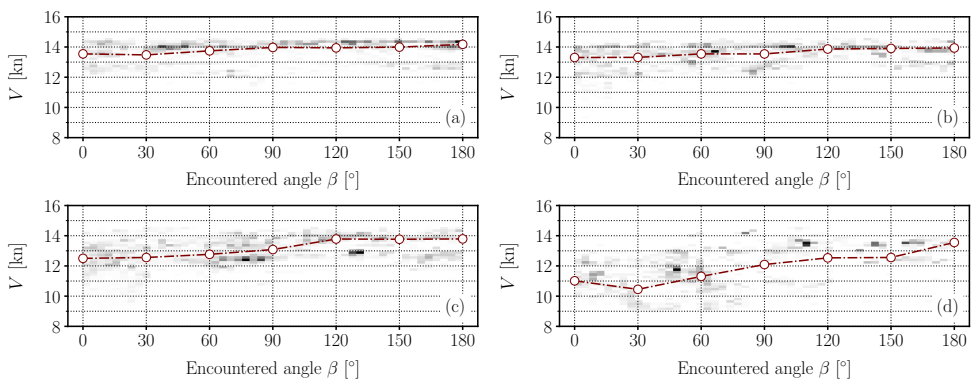

Figure 3.2: Heatmap and averaged measure speed V_{real} in terms of the wave heading angle β for the studied chemical tanker for (a) BN-3, (b) BN-4, (a) BN-5, and (b) BN-6.

The relative wave heading angles β of approximately 0°, 30°, 60°, 90°, 120°, 150°, and 180° are selected as the reference wave headings for comparison purposes. To increase

the sample size of sailing conditions located at each wave heading span, the specific angles β are collected in the range of $\pm 5°$; for instance, $85° \sim 95°$ is represented as 90°. Notably, the measurement data with relative wave angles between $0° \sim 10°$ and $170° \sim 180°$ are considered head seas and following seas, respectively. Figure 3.2 presents the heatmaps of the measured speeds versus the encountered wave heading angles, and these can help with visualizing how V_{real} changes as β increases from a head sea to a following sea. All sailing speeds of a ship under each Beaufort scale and within each specific relative wave angle span are averaged to represent the measured (mean) speed for that sea condition. The red circle markers are the obtained averaged speeds used for the verification process. The full-scale measured V_{real} is significantly scattered along the averaged lines in the heatmaps.

For semi-empirical model verification in head waves, the PCTC and the chemical tanker are employed as the case study ships. The studied power settings are approximately 8800 kW (60% MCR) for the PCTC and 4300 kW (52% MCR) for the chemical tanker.

3.4.2 Machine learning model

When the XGBoost machine learning method is used to construct a ship's speed-power performance model, more than 3 months of raw data containing operational and navigational information collected onboard a PCTC are used for both model training and testing. There are different types of measurement noise in the measured raw data. For ship operation and performance monitoring, the different measurement devices should communicate with a server to store the data. The interruptions, i.e., data transfer delays, server latency, or other communication channel conflicts between the measurement sensors and server, may prevent the data logger from accessing the data stream. The recorded nonuniform spacing of data in time is referred to as time vector jumps. The first step in the modeling process is to detect the time vector jumps in the data and synchronize the signals from different measurement devices. The obvious outliers are then detected based on some basic physical constraints, e.g., the measured propulsion power should be positive and less than the maximum continuous rating, and the measured speed cannot exceed the maximum service speed or be less than zero. In addition, repeated values and drop-outs (0 or NaN) should be excluded. The ship data obtained during the ship's maneuvering periods, such as acceleration, deceleration and course changes, are also removed from the dataset.

The other nonphysical phenomena are related to the spikes in the measurement data. These spikes are sudden changes that significantly deviate from the closed continuous data. The spikes can cause problems during the model training process. The machine learning algorithm cannot recognize these spikes, and this leads to

an incorrect description of the model. Therefore, spike values are also detected and excluded by a low-pass filter and a running standard deviation. For instance, some spikes are observed in the measured propulsion power in this study. This kind of power increase is a standard soot-blowing procedure conducting to clean the turbocharger during operations. See Figure 3.3 for a visualization of one-period propulsion power spike value detection. The envelope is set as three times the running standard deviation ($\pm 3\sigma$). The measurements that deviate from the upper and lower boundaries are excluded for further feature engineering and model training.

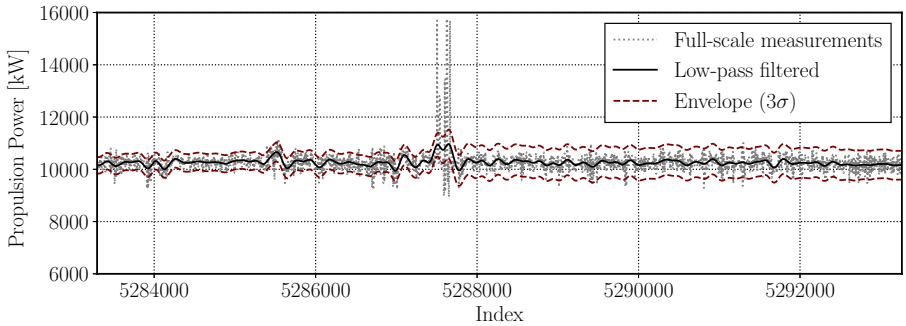

Figure 3.3: Extracted measured propulsion power with an envelope of $\pm 3\sigma$ relative to the low-pass filter for spike value detection.

CHAPTER 4

Results

This chapter presents a summary of the appended papers, including research activities and a selection of the important results, and highlights the main achievements.

4.1 Summary of Paper I

"A semi-empirical model for ship speed loss prediction in head seas and its validation with full-scale measurements"

Paper I proposes a semi-empirical speed-power model for estimating a ship's speed loss in a head sea. In particular, semi-empirical formulas to estimate added resistance due to head waves are further developed based on some state-of-the-art methods. The semi-empirical model not only provides accurate speed loss predictions but also performs fast calculations. The added resistance formulas are derived in Section 2.3 by combining the further developed NMRI formulas for resistance due to wave reflections and the improved semi-empirical models from Jinkine and Ferdinande (1974) for resistance due to wave motions. The improved semi-empirical models are verified by abundant published experimental data regarding regular head waves; see Table 3.1 in Section 3.1 for the types of applied ships. The PCTC worldwide sailing and the chemical tanker in Section 3.2 are deployed to verify the full-scale measurements.

The proposed formula for added resistance due to waves achieves sufficiently accurate approximations compared to those of the other two existing well-known approaches, i.e., the ITTC-STA2 and NTUA approaches (ITTC, 2014; Liu et al., 2016), for the

verification with regular head waves. Some typical cases are presented in Figure 4.1.

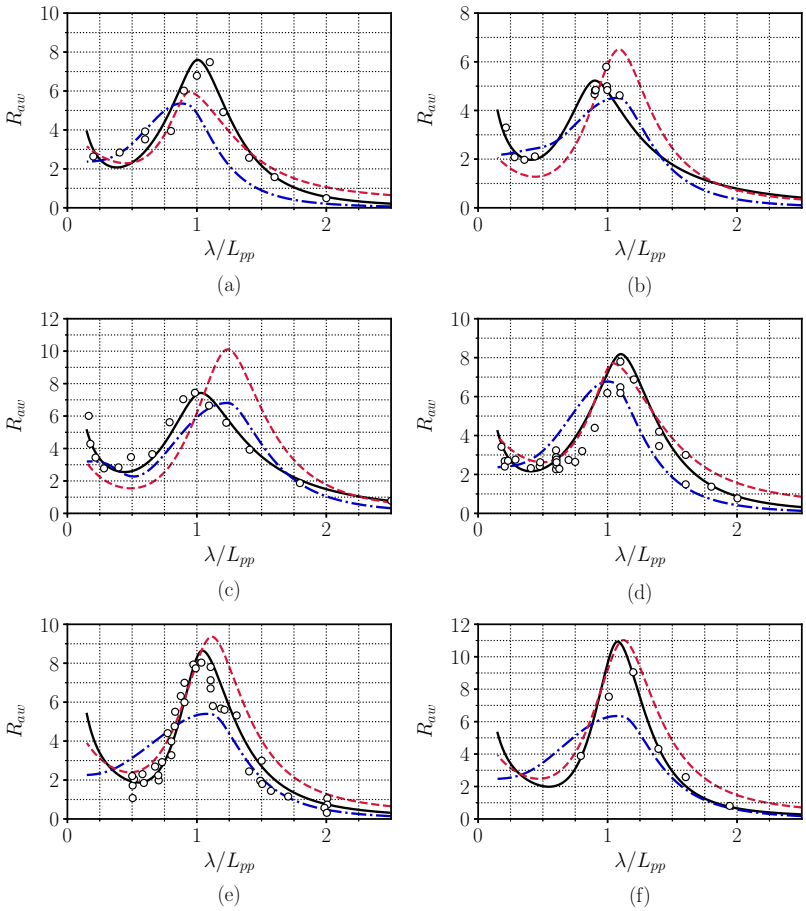

Figure 4.1: Added resistance in a regular head sea, ○ experimental data, ——— CTH, -·-·- ITTC-STA2, - - - - NTUA; estimated for (a) Bulk carrier with $F_n = 0.010$, (b) DTC container ship with $F_n = 0.139$, (c) HSVA cruise ship with $F_n = 0.232$, (d) KVLCC2 tanker with $F_n = 0.142$, (e) S175 container ship with $F_n = 0.200$, and (f) S.A. Van Der Stel with $F_n = 0.250$.

Figure 4.1 (c) presents the verification and comparison for the HSVA cruise ship model test at $F_n = 0.232$. The proposed method (denoted as CTH) significantly improves the nondimensional added resistance R_{aw} estimation for increases in resistance in the $\lambda/L_{pp} < 0.5$ short wave region and for amplitude matching at the resonance state in the long wave field. The magnitudes of the resonance resistance for the bulk carrier in Figure 4.1 (a) and the S175 container in Figure 4.1 (e) indicate that the developed formula results in better predictions than those of other methods.

Although the rest of the examples exhibit similar prediction performances in the resonance zone, the CTH formula enhances the fit with regard to increases in added resistance tail of the short wave region; see Figure 4.1 (b) for the DTC container ship and Figure 4.1 (d) for the KVLCC2 container ship.

Table 4.1: MSE analysis of all experimental measurement verification cases for regular head waves; all outcomes are normalized by the proposed formula results.

Ship type	Froude number	CTH	NTUA	ITTC-STA2	Best fit
S175 container	0.150	1	2.34	4.84	CTH
	0.200	1	3.90	3.26	CTH
	0.250	1	1.82	2.86	CTH
	0.275	1	1.23	12.99	CTH
KVLCC2 tanker	0.050	1	3.28	9.40	CTH
	0.090	1	1.19	3.91	CTH
	0.142	1	1.02	2.77	CTH
	0.180	1	1.10	3.01	CTH
DTC container	0.052	1	1.69	5.63	CTH
	0.139	1	4.15	2.20	CTH
HSVA cruise	0.166	1	6.70	1.11	CTH
	0.232	1	17.11	5.29	CTH
S.A. Van Der Stel	0.150	1	0.27	1.52	NTUA
	0.200	1	0.38	4.00	NTUA
	0.250	1	2.15	2.65	CTH
	0.300	1	1.66	3.40	CTH
Bulk carrier	0.000	1	5.61	2.62	CTH
	0.005	1	0.77	0.74	ITTC-STA2
	0.010	1	2.15	5.75	CTH
	0.150	1	1.19	6.33	CTH
Series 60 model 4210	0.266	1	5.81	6.67	CTH
	0.283	1	1.54	1.33	CTH
Series 60 model 4211	0.237	1	2.13	5.79	CTH
	0.254	1	4.67	4.73	CTH
Series 60 model 4212	0.207	1	3.50	10.32	CTH
	0.222	1	3.08	3.61	CTH
Series 60 model 4213	0.177	1	1.37	3.43	CTH
	0.195	1	1.03	2.52	CTH
Series 60 model 4214	0.147	1	0.96	1.83	NTUA
	0.165	1	1.03	1.48	CTH

The mean squared error (MSE) is used to evaluate the quality of all numerical predictions from a quantitative assessment viewpoint (Hastie et al., 2009). All assessment results are listed in Table 4.1. The MSEs of the ITTC-STA2 and NTUA results are normalized by the values of the predicted values output by the CTH method. As Table 4.1 expresses, the proposed formula has the best prediction performances for almost all the studied instances, except for 3 cases with the NTUA approach and 1 case with the ITTC-STA2 formula. The introduced formula demonstrates superior estimation ability compared with those of the other widely used methods in regular head sea conditions. Accordingly, these results are considered to be sufficient for the calculation of wave-induced added resistance.

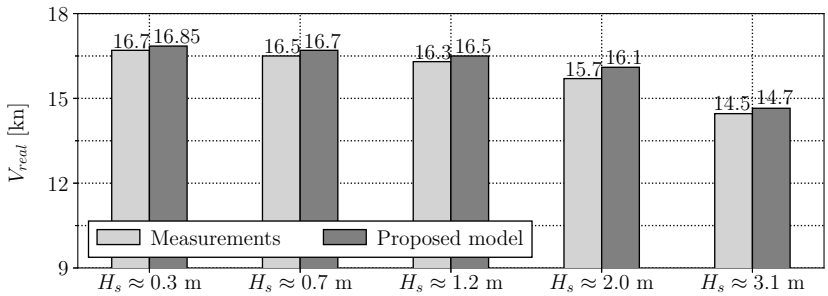

Figure 4.2: The real speed comparison for the PCTC case study with various sea conditions estimated for an engine power setting of approximately 8800 kW.

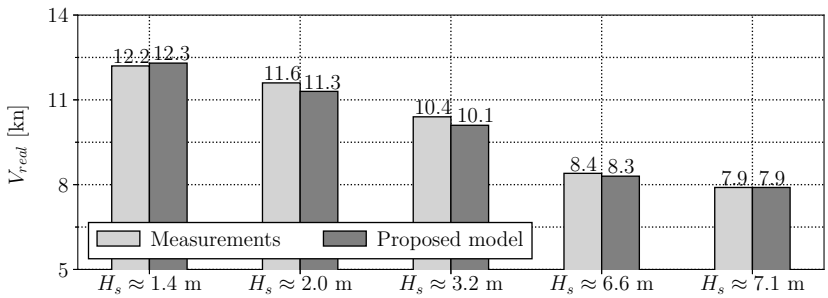

Figure 4.3: The real speed comparison for the chemical tanker case study with various sea conditions estimated for an engine power setting of approximately 4300 kW.

The proposed semi-empirical speed-power model is then verified with a comparison of the ship's real speed V_{real}. When assessing a ship's real speed with real encountered wind and wave conditions, the power setting should be fixed near a specific value. The postprocessed full-scale measurements with engine powers of approximately 8800 kW (60% MCR) for the PCTC and 4300 kW (52% MCR) for the chemical tanker are chosen as the power settings for the speed loss verification process. All the measurements and the theoretical real ship speed estimations around a specific significant

wave height are averaged for a comparison between the calm and harsh weather results. The values of V_{design} at the defined engine power settings are 16.9 kn and 12.8 kn for the PCTC and tanker, respectively.

As Figure 4.2 illustrates, the proposed model produces consistently excellent predictions through all considered wave conditions for the studied PCTC, with a maximum discrepancy of approximately 0.2 kn. The largest speed loss is approximately 2.4 kn at $H_s = 3.1$ m, i.e., a 14% involuntary speed reduction caused by the encountered wave and wind conditions. Satisfactory accuracy is also observed for the chemical tanker in Figure 4.3, where the verification cases start from $H_s \approx 1.4$ m in harsh sea conditions with a significant wave height greater than 7 m ($4.5 < H_s < 5.5$ m is skipped because too few measurements exist in that range). The model estimations have slight fluctuations compared to the corresponding measurements, but they are still in good agreement.

4.2 Summary of Paper II

"A practical speed loss prediction model at arbitrary wave heading for ship voyage optimization"

In this study, the semi-empirical speed-power model developed for the head sea in Paper I is further developed to estimate a ship's speed loss due to waves from arbitrary angles. In this model, formulas to estimate the added resistance are further developed to consider waves from different angles. The improved formulas are verified by experimental data from 5 ships encountering regular waves. They achieve reasonable accuracy with a high calculation speed. The proposed model is then applied for speed loss prediction and compared to the well-known Kwon (2008) method. The PCTC, chemical tanker, and container ship in Section 3.2 are employed as the case study ships. The impact of such an improved speed loss prediction model on a ship's voyage optimization is also investigated.

Figure 4.4 shows one instance of the nondimensional added resistance R_{aw} verification for the HSVA cruise ship, where the nondimensional reflection-induced resistance R_{awr} and nondimensional ship motion-induced resistance R_{awm} are illustrated as well. The experiment is conducted from 30° to 180°at a Froude number of $F_n = 0.232$. The proposed formula is in good agreement with the measurements for 30° and 60°, for both the tail increase in the extreme short wave region and peak value seizing for the resonance position. Although some fluctuations exist for the other considered angles, the results can still catch up with the measurement trend. The peak value decreases and moves to the lower wavelength (λ/L_{pp}) region as the relative wave

angle increases. The negative resistance on the ship stern caused by the reflections of the following waves is captured.

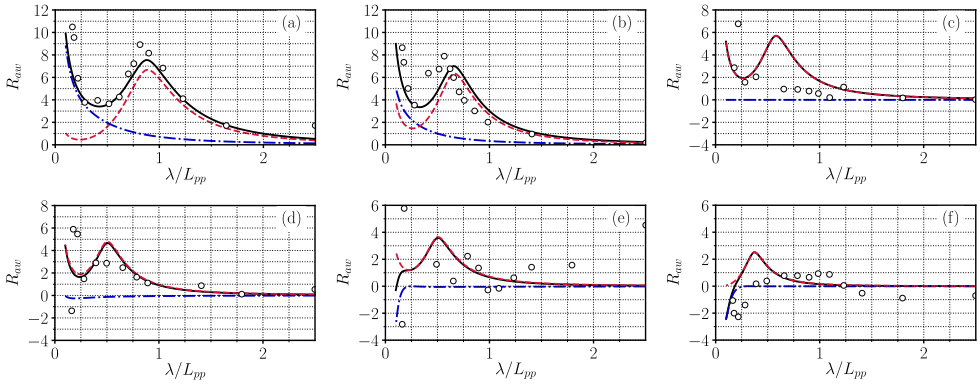

Figure 4.4: Added resistance for the HSVA cruise due to regular waves with arbitrary angles at $F_n = 0.232$, ○ experimental data, —— R_{aw}, -·-·- R_{awr}, - - - - R_{awm}; estimated at (a) 30 degrees, (b) 60 degrees, (c) 90 degrees, (d) 120 degrees, (e) 150 degrees, and (f) 180 degrees.

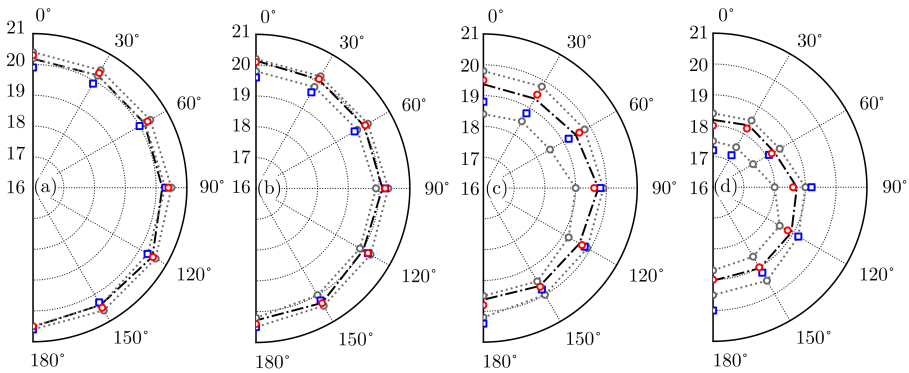

Figure 4.5: The speed loss estimation results output by both Kwon's method and the proposed model in comparison with the measurements obtained for the case study container ship, ○ proposed model prediction, □ Kwon's method prediction, ····· ship real speed V_{real} upper and lower bound for the piecewise boundary of each Beaufort scale H_s, -·-·- average of real measurements; estimated for (a) BN-4, (b) BN-5, (c) BN-6, and (d) BN-7.

For the speed-power model application, the speed losses predicted by the proposed model are consistently in good agreement with the full-scale measurements. Especially for chemical tankers, the widely used Kwon (2008) method cannot provide

reasonable values. The predicted values always fluctuate around the baseline. Moreover, the Kwon (2008) method can only give one speed prediction for a specific Beaufort number. However, the significant wave height H_s varies greatly along the Beaufort scale. 4.5 represents the container ship's speed estimation. The proposed model results in the best average real speed V_{real} predictions (in black circle markers), as they coincide with the real measurements. This model can also provide highly realistic and precise speed loss estimations for the upper and lower bounds for each Beaufort-scale wave condition; this is because the proposed model can predict the speed loss for a sea state with specific metocean parameters, such as H_s, T_z, etc. The gray dotted lines in Figure 4.5 (c) represent speeds evaluated using the measurement data close to the piecewise boundary of the considered Beaufort scale, such as 2.5 m and 4.0 m for the BN-6 condition.

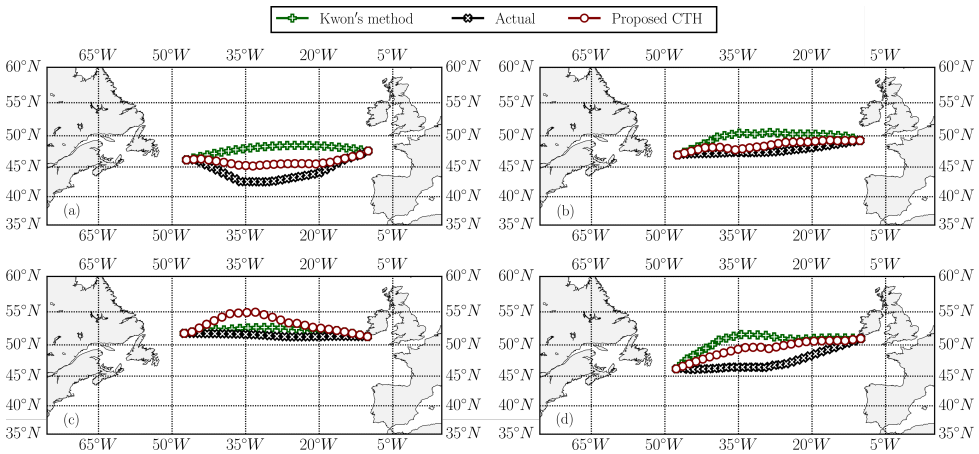

Figure 4.6: Optimal trajectories for the selected case study: (a) voyage 2009-01-18, (b) voyage 2009-02-18, (c) voyage 2009-12-26, and (d) voyage 2010-01-13.

The proposed model and Kwon (2008) method are then implemented for voyage optimization. Four winter voyages in an open sea area, on 2009-01-18 and 2009-12-26 for the eastbound direction and on 2009-02-18 and 2010-01-13 for the westbound direction, are used to demonstrate the importance of an accurate ship speed-power model. In the voyage optimization analysis, the three-dimensional Dijkstra's algorithm (Wang et al., 2019) is applied for highly flexible speed adjustment and route planning. The aforementioned relatively unstable prediction ability of the Kwon (2008) method also leads to significant variance in the voyage optimization results, both for the final optimized trajectories and the optimal ship speed. Figure 4.6 presents the optimized trajectories for those selected routes based on the proposed model and Kwon (2008) method. The results show that the different models have varying effects on voyage optimization, and the optimal trajectories differ significantly

for instances in the open sea.

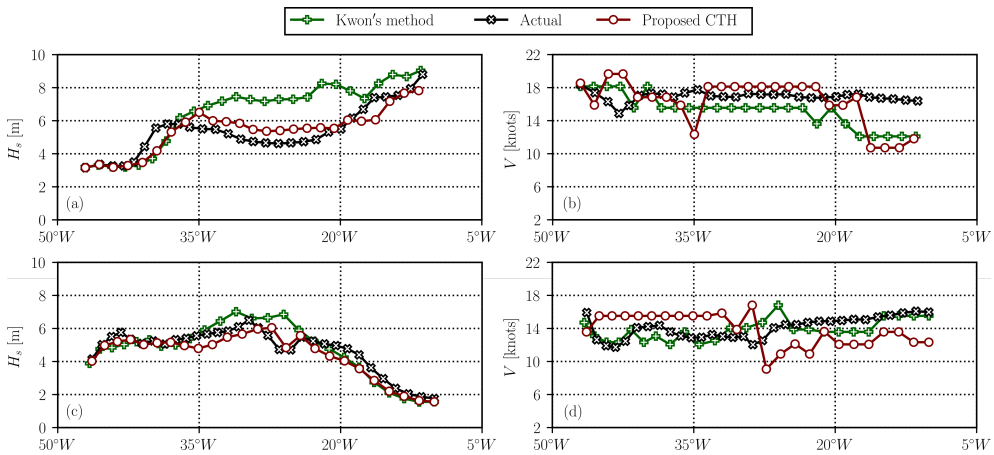

Figure 4.7: The encountered significant wave heights H_s and ship speeds V along the optimized and actual ship routes for the two case study voyages. (a) H_s along voyage 2009-01-18, (b) V along voyage 2009-01-18, (c) H_s along voyage 2010-01-13, and (d) V along voyage 2010-01-13.

The encountered significant wave heights H_s and ship speeds V, along with two optimized ship voyages and the actual voyages, i.e., the eastbound voyage 2009-01-18 and the westbound voyage 2010-01-13, are presented in Figure 4.7. The maximum discrepancy of the encountered H_s for voyage 2009-01-18 is almost 2 meters. The voyage optimization results obtained using the proposed model recommend a sailing speed of 2 knots faster than that suggested by optimization with Kwon (2008) method between the $35°W$ and $20°W$ areas to avoid encountering high sea environments. When the ship encounters a large H_s above 6 m, the voyage optimization results using our proposed model recommend slowing down considerably to decrease the added resistance due to waves. A similar difference can also be observed for voyage 2010-01-03, in which the route optimized by Kwon (2008) method encounters harsher wave conditions. In contrast, the route navigated by the proposed model adjusts the speed to allow the ship to sail in the calmest possible wave conditions.

4.3 Summary of Paper III

"XGBoost method to model a ship's propulsion power in seaways"

With the development of sensor technology and its wide exploitation in the shipping industry, a large amount of ship performance-related data is collected onboard ships, and this provides new opportunities to better model a ship's actual energy

performance when sailing at sea. In this study, a machine learning method, i.e., the XGBoost method, is used to build models for predicting a ship's propulsion power in various operational and metocean conditions. The speed-power models are trained in 2 scenarios: 1) ship operational profiles and metocean conditions are used as feature inputs and 2) ship motions are used instead of the encountered metocean parameters as inputs. For each scenario, two power prediction models are established by the XGBoost method and compared afterwards. The first performance model is trained by setting the measured propulsion power as the training target, while the second model is trained by setting the increase in propulsion power due to the encountered sea environments as the training target. In the second model, a ship's baselines obtained from experimental tests and sea trials are assumed to be available for estimating the propulsion power of the ship in calm water conditions. Then, the target of the machine learning method is to model the power increase (the difference between the measured power and calm water baseline $P_{measurement} - P_{calm}$). The full-scale measurements of the PCTC presented in Section 3.2 are applied for this study. The root mean square error (RMSE) and the coefficient of determination (R^2) are calculated as references for describing the generalization capability of the constructed models.

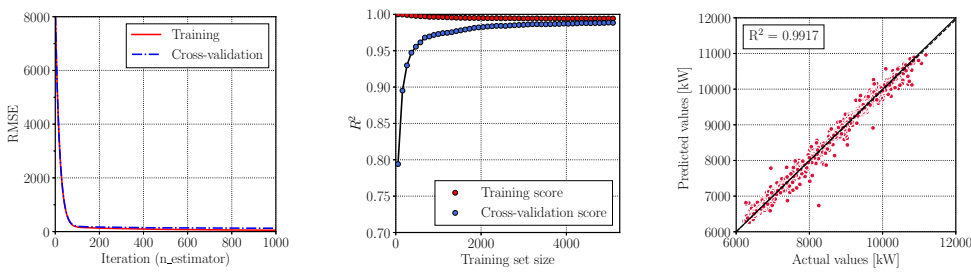

Figure 4.8: Learning curve for the load-based XGBoost machine learning model (without baseline) training process in a metocean environment: (a) RMSE, (b) coefficient of determination R^2, and (c) correlations between the predicted ship propulsion power values and the actual measurements.

The amount of power required in calm water relies on the experimental baselines of the ship speed and draft. The drafts at the stern and stem were measured once per day for the case study PCTC. The frequency is much lower than those of the other training measurements (1 Hz). Uncertainties and noise are inevitably introduced into the training data when subtracting the calm water power from the measured propulsion power. Thus, for metocean environment-based machine learning models, the model choosing the power increase as the training target yields slightly lower power predictions than those of the other models. Figure 4.8 (a) and Figure 4.8 (b) present the learning curves of the RMSE and R^2 for cross-validation of the training

process, respectively. The small discrepancies between the training scores and cross-validation scores indicate that the hyperparameters chosen minimize overfitting. The predicted power versus the measured power for the testing set is shown in Figure 4.8 (c). The R^2 is 0.9917 and indicates a satisfactory prediction performance.

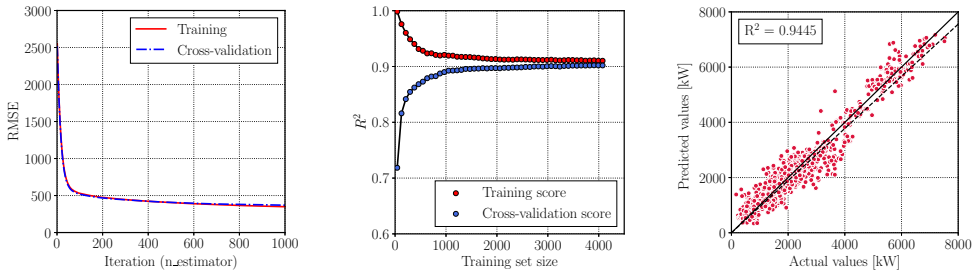

(a) **(b)** **(c)**

Figure 4.9: Learning curve for the ship motion velocity response with the baseline XGBoost machine learning model training process: (a) coefficient of determination R^2, (b) RMSE, (c) correlations between the predicted ship propulsion power values and the actual measurements.

In scenario 2, in addition to the original 6 DOF motions, the 1st-order derivative and 2nd-order derivative of the ship motions, i.e., the motion velocity and motion acceleration, respectively, are implemented as feature inputs to consider the effect of ship motions on a ship's performance models. The mean value, standard deviation, skewness and kurtosis are estimated to describe the motion statistics and are applied as the training features. For different feature inputs, the power increases as training targets yield better performance predictions. A ship's motion response is linearly dependent on the encountered wave amplitudes (despite extreme conditions such as storm and green water influence), while added resistance due to waves is estimated as a quadratic function in terms of the wave amplitudes. The 1st-order derivative of ship motion, i.e., motion velocity, has the strongest correlation with the wave-induced power increase. Thus, the motion velocity case achieves the highest R^2 score; see Figure 4.9 for the learning curve and testing set evaluation. The testing R^2 score of the motion-based model is relatively lower than that of the metocean-based model. The low score of the motion-based model may be due in part to the time interval being selected as a stationary sea state for the data inputs of the training process.

The proposed metocean-based model (with original propulsion power as the target) is further implemented for comparison with the measured power and conventional semi-empirical models with regard to the prediction of fuel consumption and sailing time within one voyage. It should be noted that the conventional method in ITTC (2014) adopted the theoretical model of added resistance, without resistance and

power correction factors. Two voyages are used as case studies in this analysis. The proposed machine learning model's prediction results fluctuate slightly compared to real measurements, but they are in good agreement overall. Due to the fact that it underestimates the resistance and power, the semi-empirical model has a prediction gap of up to 30000 kWh for the power accumulation during voyage 1 in Figure 4.10 and 4 hours for the sailing time accumulation during voyage 2 in Figure 4.11.

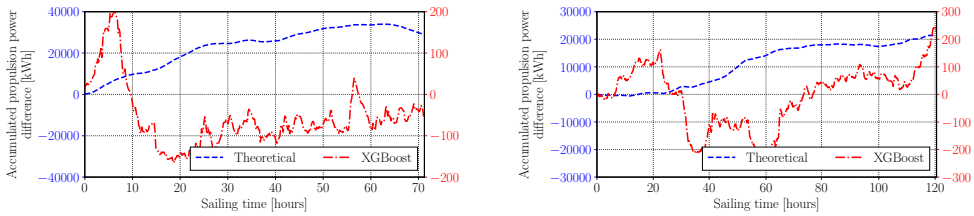

(a) Voyage 1 **(b)** Voyage 2

Figure 4.10: The accumulated propulsion power differences calculated by the proposed XGBoost machine learning speed-power model and the theoretical method for voyage 1 and voyage 2.

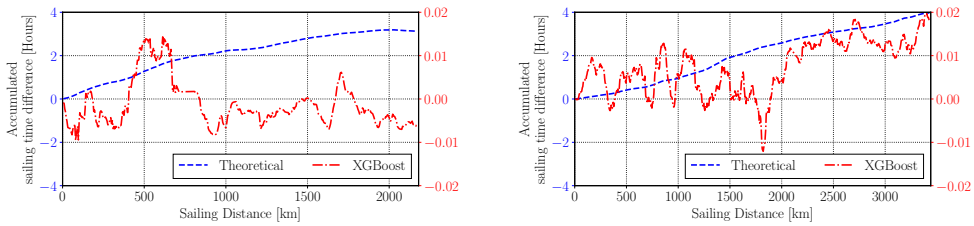

(a) Voyage 1 **(b)** Voyage 2

Figure 4.11: The accumulated sailing time differences obtained by the proposed XGBoost machine learning speed-power model and the theoretical method for voyage 1 and voyage 2.

Finally, it is concluded that the XGBoost machine learning method can construct an accurate speed-power model for a ship in actual sailing environments based on its onboard measurements.

CHAPTER 5

Conclusions

In this thesis, two types of speed-power performance models, i.e., a semi-empirical model (white box) and big data-driven machine learning models (black box), are developed to predict a ship's propulsion power in an actual sailing environment at sea, especially for the task of voyage optimization. The semi-empirical model is able to predict a ship's propulsion power within a $5\% \sim 10\%$ difference compared to the real measurements, and the discrepancies of the results output by the machine learning model are less than 1%. It is concluded that when a large amount of ship operation data is available, the machine learning method is recommended to establish the ship speed-power model for voyage optimization. Otherwise, the semi-empirical model should be adopted since it needs limited input data regarding the ship characteristics. The main findings and conclusions are presented below with respect to the subtasks in Section 1.3.

The development of a semi-empirical model for head waves

The semi-empirical model for head waves in Paper I includes improved semi-empirical formulas for added resistance due to regular waves. Based on a quantitative assessment via a statistical MSE analysis, this model produces the best approximations for almost all the collected published experimental data for regular waves compared to those output by the well-known ITTC-STA2 and NTUA methods (ITTC, 2014; Liu et al., 2016). The formulas combine the further developed NMRI formulas (Tsujimoto et al., 2008) for short waves (due to wave reflections) and the improved semi-empirical models from Jinkine and Ferdinande (1974) for long waves (due to wave motions). It

is shown that the proposed model provides consistently excellent ship speed predictions in real seaways, with maximum discrepancies of 0.4 kn (2.5%) for the PCTC and 0.3 kn (2.9%) for the chemical tanker.

The extension of the semi-empirical model to arbitrary wave headings

The semi-empirical model in Paper I is extended to arbitrary wave headings in Paper II. The model for arbitrary wave headings is based on the extension of the formulas for head waves. The formulas can be calculated quickly by using as few ship characteristics as possible while still achieving good accuracy. The full-scale measurements from three case study ships, i.e., a PCTC, a container ship, and a chemical tanker, are employed to verify the proposed semi-empirical speed-power model for speed loss prediction. It is shown that the proposed model has better ship speed prediction capability than that of the widely used Kwon (2008) method. To quantify this improvement, for the blunt ship, i.e., the chemical tanker, the proposed model yields an approximately 40% increase in speed prediction accuracy in bow seas under BN-6 weather conditions. The increases are as high as 7% for the PCTC (BN-6) and 6% for the container ship (BN-7). Notably, the semi-empirical model is only developed and verified under the design load condition.

The machine learning model for ship speed-power performance

The XGBoost algorithm is deployed to establish the machine learning-based speed-power model for the PCTC in Paper III, and it does so by using the full-scale measurement data from the onboard monitoring system of the ship. The establishment of the model consists of two scenarios. In scenario 1, the metocean environmental loads and ship operation parameters are selected as the input features, and the XGBoost system is trained to predict the propulsion power. In scenario 2, instead of using the metocean data, the recorded ship's 6 DOF motion responses, the related motion velocity (1st order derivative) and the acceleration (2nd order derivative) are deployed as inputs. It is shown that the metocean-based machine learning model with the target of measured propulsion power results in less than a 1% discrepancy compared to the real measurements in the testing dataset. Then, this model is implemented for the estimation of the ship's actual speed. Except for the following wave condition (due to a lack of data), the predicted speeds are in good agreement with the measured data, within a 0.1 kn (up to 0.4%) difference. The machine learning model is trained by using data from different stationary sea states. Individual stationary sea states during short-term navigation cannot be considered.

The impacts of various speed-power models on voyage optimization

In Paper II, the proposed semi-empirical and Kwon (2008) models are implemented in voyage optimization systems to investigate the influences of different speed-power models. Significant impacts on the voyage optimization results, such as the sailing distances, trajectories, sailing speeds, and encountered sea environments, are observed due to the different models. It is shown that the proposed model recommends a faster sailing speed to avoid severe wave conditions (maximum 20% H_s decrease), leading to reduced fuel consumption.

The benefit of the proposed speed-power models for voyage optimization

The metocean-based machine learning model is implemented in the individual voyage propulsion power and sailing time accumulation studies in Paper III. For 72 hours and 120 hours of sailing, it was determined that the proposed machine learning model can dramatically reduce the accumulated propulsion power difference by up to ten times more than the semi-empirical model (without the wave height correction factor). An increase in prediction accuracy of up to 4% is also found for the sailing time accumulation difference.

CHAPTER 6

Future work

The main objective of this thesis is to develop ship speed-power performance models that can describe a ship's power/fuel consumption performance, or reversely estimate a ship's real sailing speed in seaways (speed reduction caused by encountered sea environment conditions). These models should be sufficiently accurate for application in a ship's voyage optimization system. For this special application case, both semi-empirical performance models and big data-driven machine learning models have been developed and verified by experimental and full-scale measurement data. The semi-empirical models can allow for fast computation of a ship's energy performance for voyage optimization. Since the parameters in the semi-empirical models are (in principle) obtained by regression, these models may provide accurate expected speed loss values for ships of the same type. However, for an individual ship, the semi-empirical models may lead to large scattering of the ship's performance predictions. To best model a ship's energy performance, it is important to consider the ship's actual performance when sailing at sea, i.e., the full-scale measurements collected for the specific ship of interest. In this way, the machine learning method can play an important role in the further development of ship performance models. In addition to a ship's energy performance-related parameters, the full-scale measurement data also contain other relevant information, such as different sea parameters, motion responses, or structural responses, that can have a direct potential impact on a ship's performance. Therefore, my future research plan is to exploit the capabilities of machine learning methods and the collected big data for improving a ship's performance model as well as for other related applications.

Further improvements in the speed-power performance models

The proposed semi-empirical model can be further verified by different ships if additional full-scale measurements are available. Especially for the wave height-based ship resistance and power increase correction factor, this is a preliminary idea for calibrating the model. A thorough investigation with additional experimental tests and full-scale measurements of ships should be conducted to configure a more flexible formula for this factor based on various input parameters. The developed semi-empirical models provide reliable mean performances for full-scale measurements over several months or over years. They can act as a baseline for an increasingly dynamic propulsion prediction model for a ship in the short term (one voyage). The dynamic model is driven by some time series analysis algorithms to increase the short-term accuracy of 'online performance predictions for a ship under a stationary sea state. In addition, machine learning methods will be introduced in the modeling process to integrate ship-specific parameters in the proposed semi-empirical models.

Extended applications of machine learning methods

The applicability of machine learning methods can be widened by using more options to study ship fatigue for safety purposes. Machine learning techniques can be used to model the relationships between the encountered wave conditions, ship operation profiles and measured stress responses. The calculated fatigue damage can be verified by the high-cycle fatigue principle and spectral fatigue method for long-term (several years) and short-term (one voyage) navigation.

Any maritime-related studies and innovations need to know a ship's actual encountered wave environments. These are used as inputs for developing and optimizing some measures to improve a ship's safety and energy efficiency. Large investments, e.g., satellites, onboard radar, blue green lidar, etc., have been adopted to obtain increasingly reliable sea weather environments. However, the accuracy of such measures is still not satisfactory for shipping-related activities. It would be interesting to implement an inverse machine learning method to obtain a ship's sea environments through its motions and other response parameters when sailing at sea.

References

Alexandersson, M. (2009). *A study of methods to predict added resistance in waves* (MSc thesis). Royal Institute of Technology, Sweden.

Bal Beşikçi, E., Arslan, O., Turan, O., & Ölçer, A. (2016). An artificial neural network based decision support system for energy efficient ship operations. *Computers & Operations Research*, *66*, 393–401.

Ballou, P. J. (2013). Ship energy efficiency management requires a total solution approach. *Marine Technology Society Journal*, *47*(1), 83–95.

Boese, P. (1970). Eine einfache methode zur berechnung der widerstandserhöhung eines schiffes im seegang. *Schriftenreihe Schiffbau*, *258*, 1–9.

Boom, H., Huisman, H., & Mennen, F. (2013). New guidelines for speed/power trials level playing field established for imo eedi. *SWZ Maritime*.

Carlton, J. (2012). *Marine propellers and propulsion (4th edition)*. Butterworth-Heinemann.

Chen, T., & Guestrin, C. (2016). XGBoost: a scalable tree boosting system. *Proceedings of the 22nd ACM SIGKDD International Conference on Knowledge Discovery and Data Mining*, 785–794.

CMEMS. (2019). *E.U. Copernicus Marine Service Information*. Retrieved May 18, 2019, from http://marine.copernicus.eu/

Copernicus. (2019). *Copernicus Climate Change Service (C3S): ERA5: Fifth generation of ECMWF atmospheric reanalyses of the global climate*. Retrieved May 16, 2019, from https://cds.climate.copernicus.eu/cdsapp#!/home

Coraddu, A., Oneto, L., Baldi, F., & Anguita, D. (2015). Ship efficiency forecast based on sensors data collection: Improving numerical models through data analytics. *OCEANS 2015 - Genova*, 1–10.

DNV GL. (2015). *Energy management study 2015* (tech. rep.). Hamburg, Germany. https://www.dnvgl.com/

el Moctar, O., Shigunov, V., & Zorn, T. (2012). Duisburg test case: post-panamax container ship for benchmarking. *Ship Technology Research*, *59*(3), 50–64.

Faltinsen, O. M., Minsaas, K. J., Liapis, N., & Skjordal, S. O. (1980). Prediction of resistance and propulsion of a ship in a seaway. *Proceedings of the 13th Symposium on Naval Hydrodynamics*, 505–529.

Friedman, J., Hastie, T., & Tibshirani, R. (2000). Additive logistic regression: a statistical view of boosting (With discussion and a rejoinder by the authors). *The Annals of Statistics*, *28*(2), 337–407.

Fujii, H., & Takahashi, T. (1975). Experimental study on the resistance increase of a large full ship in regular oblique waves. *Journal of the Society of Naval Architects of Japan*, *1975*(137), 132–137.

GEBCO. (2019). *GEBCO 2019 Grid*. Retrieved May 20, 2019, from https://www.gebco.net/data_and_products/gridded_bathymetry_data/#a1

Gerritsma, J., & Beukelman, W. (1972). Analysis of the resistance increase in waves of a fast cargo ship. *International Shipbuilding Progress*, *19*(217), 285–293.

Grin, R. (2012). On the prediction of wave added resistance. *Proceedings of 11th International Marine Design Conference*.

Guo, B. J., & Steen, S. (2011). Evaluation of added resistance of kvlcc2 in short waves. *Journal of Hydrodynamics*, *23*(6), 709–722.

Hasselmann, K., Barnett, T. P., Bouws, E., Carlson, H., Cartwright, D. E., Enke, K., Ewing, J. A., Gienapp, H., Hasselmann, D. E., Kruseman, P., Meerburg, A., Muller, P., Olbers, D. J., Richter, K., Sell, W., & Walden, H. (1973). Measurements of wind-wave growth and swell decay during the joint North sea wave project (JONSWAP). *Ergnzungsheft zur Deutschen Hydrographischen Zeitschrift Reihe*.

Hastie, T., Tibshirani, R., & Friedman, J. (2009). *The elements of statistical learning (2nd edition)*. Springer.

Havelock, T. (1942). The drifting force on a ship among waves. *The London, Edinburgh, and Dublin Philosophical Magazine and Journal of Science*, *33*(221), 467–475.

Holtrop, J., & Mennen, G. (1982). An approximate power prediction method. *International Shipbuilding Progress*, *29*(335), 166–170.

IMO. (2011). Amendments to the annex of the protocol of 1997 to amend the international convention of pollution from ships, 1973, as modified by the protocol of 1978 relating thereto. *MEPC.203(62)*.

IMO. (2020). Reduction of GHG emissions from ships, fourth IMO GHG study 2020 – final report. *MEPC 75/7/15*.

ISO. (2015). Ships and marine technology - guidelines for the assessment of speed and power performance by analysis of speed trial data. *15016*.

ITTC. (2002). Resistance uncertainty analysis example for resistance test. *Recommended procedures 7.5-02-02-02*.

ITTC. (2014). Analysis of speed/power trial data. *Recommended procedures and guidelines 7.5-04-01-01.2*.

ITTC. (2017). Seakeeping experiments. *Recommended procedures and guidelines 7.5-02-07-02.1*.

ITTC. (2018). Calculation of the weather factor f_w for decrease of ship speed in wind and waves. *Recommended Procedures and Guidelines 7.5-02-07-02.8*.

Jinkine, V., & Ferdinande, V. (1974). A method for predicting the added resistance of fast cargo ships in head waves. *International Shipbuilding Progress*, *21*(238), 149–167.

Journée, J. (2001). *Verification and validation of ship motions program SEAWAY*. Delft University of Technology Ship hydromechanics Laboratory, Report1213a.

Kadomatsu, K. (1988). *Study on the required minimum output of main propulsion engine considering maneuverability in rough sea* (Doctoral dissertation). Yokohama National University, Japan.

Kim, D., Lee, S., & Lee, J. (2020). Data-driven prediction of vessel propulsion power using support vector regression with onboard measurement and ocean data. *Sensors*, *20*(6), 1588.

Kuroda, M., Tsujimoto, M., Fujiwara, T., Ohmatsu, S., & Takagi, K. (2008). Investigation on components of added resistance in short waves. *Journal of the Japan Society of Naval Architects and Ocean Engineers*, *8*, 171–176.

Kwon, Y. J. (2008). Speed loss due to the added resistance in wind and waves. *The Naval Architect*, 14–16.

Lang, X., & Mao, W. (2020). A semi-empirical model for ship speed loss prediction at head sea and its validation by full-scale measurements. *Ocean Engineering*, *209*, 107494.

Lang, X., Wang, H., Mao, W., & Osawa, N. (2020). Impact of ship operations aided by voyage optimization on a ship's fatigue assessment. *Journal of Marine Science and Technology*.

Larsson, E., Simonsen, M., & Mao, W. (2015). DIRECT optimization algorithm in weather routing of ships. *Proceedings of the 25th International Offshore and Polar Engineering Conference*.

Leifsson, L. Þ., Sævarsdóttir, H., Sigurðsson, S. Þ., & Vésteinsson, A. (2008). Grey-box modeling of an ocean vessel for operational optimization. *Simulation Modelling Practice and Theory*, *16*(8), 923–932.

Lewis, E. V. (1988). *Principles of naval architecture (2nd edition)* (Vol. 2. SNAME). The Society of Naval Architects; Marine Engineers.

Liu, S., Shang, B., Papanikolaou, A., & Bolbot, V. (2016). Improved formula for estimating added resistance of ships in engineering applications. *Journal of Marine Science and Application*, *15*(4), 442–451.

Lu, R., Turan, O., Boulougouris, E., Banks, C., & Incecik, A. (2015). A semi-empirical ship operational performance prediction model for voyage optimization towards energy efficient shipping. *Ocean Engineering*, *110*, 18–28.

Mao, W., Lenaers, P., Salomonsson, H., & Brandholm, P. (2016a). Machine learning to predict a ship's fuel consumption in seaways. *PRADS 2016 - Proceedings of the 13th International Symposium on PRActical Design of Ships and Other Floating Structures*.

Mao, W., Rychlik, I., Wallin, J., & Storhaug, G. (2016b). Statistical models for the speed prediction of a container ship. *Ocean Engineering*, *126*, 152–162.

Maruo, H. (1957). The excess resistance of a ship in rough seas. *International Shipbuilding Progress*, *4*(35), 337–345.

Maruo, H. (1960). Wave resistance of a ship in regular head seas. *Bulletin of the Faculty of Engineering, Yokohama National University*, *9*, 73–91.

Maruo, H. (1963). Resistance in waves, research on seakeeping qualities of ships in Japan. *The Society of Naval Architects of Japan*, *8*, 67–102.

Parkes, A., Sobey, A., & Hudson, D. (2018). Physics-based shaft power prediction for large merchant ships using neural networks. *Ocean Engineering*, *166*, 92–104.

Pérez Arribas, F. (2007). Some methods to obtain the added resistance of a ship advancing in waves. *Ocean Engineering*, *34*(7), 946–955.

Petersen, J. P., Winther, O., & Jacobsen, D. J. (2012). A machine-learning approach to predict main energy consumption under realistic operational conditions. *Ship Technology Research*, *59*(1), 64–72.

Sadat-Hosseini, H., Wu, P.-C., Carrica, P. M., Kim, H., Toda, Y., & Stern, F. (2013). CFD verification and validation of added resistance and motions of KVLCC2 with fixed and free surge in short and long head waves. *Ocean Engineering*, *59*, 240–273.

Salvesen, N. (1978). Added resistance of ships in waves. *Journal of Hydronautics*, *12*(1), 24–34.

Shao, W., Zhou, P., & Thong, S. K. (2012). Development of a novel forward dynamic programming method for weather routing. *Journal of Marine Science and Technology*, *17*(2), 239–251.

Simonsen, M. H., Larsson, E., Mao, W., & Ringsberg, J. W. (2015). State-of-the-art within ship weather routing. *Proceedings of the 34th International Conference on Offshore Mechanics and Arctic Engineering - OMAE*.

Stopford, M. (2009). *Maritime economics*. London: Routledge.

Strom-Tejsen, J., Yeh, H., & Moran, D. (1973). Added resistance in waves. *Transactions of the Society of Naval Architects and Marine Engineers*, *81*, 109–143.

Takahashi, T. (1988). A practical prediction method of added resistance of a ship in waves and the direction of its application to hull form design. *Transactions of the West-Japan Society of Naval Architects*, *75*(75), 75–95.

Tillig, F., Ringsberg, J., Mao, W., & Ramne, B. (2017). A generic energy systems model for efficient ship design and operation. *Proceedings of the Institution*

of Mechanical Engineers, Part M: Journal of Engineering for the Maritime Environment, *231*(2), 649–666.

Tillig, F. (2020). *Simulation model of a ship's energy performance and transportation costs* (Doctoral dissertation). Chalmers University of Technology, Sweden.

Tillig, F., Ringsberg, J. W., Mao, W., & Ramne, B. (2018). Analysis of uncertainties in the prediction of ships' fuel consumption – from early design to operation conditions. *Ships and Offshore Structures*, *13*(sup1), 13–24.

Townsin, R. L., & Kwon, Y. J. (1982). Approximate formulae for the speed loss due to added resitance in wind and waves. *The Royal Institution of Naval Architects*, *124*, 199–207.

Tsujimoto, M., Shibata, K., Kuroda, M., & Takagi, K. (2008). A practical correction method for added resistance in waves. *Journal of the Japan Society of Naval Architects and Ocean Engineers*, *8*, 177–184.

UNCTAD. (2018). *Review of maritime transport 2018*. United Nations Publications, New York, USA.

Ursell, F., & Dean, W. R. (1947). The effect of a fixed vertical barrier on surface waves in deep water. *Mathematical Proceedings of the Cambridge Philosophical Society*, *43*(03), 374–382.

Uyanık, T., Karatuğ, Ç., & Arslanoğlu, Y. (2020). Machine learning approach to ship fuel consumption: A case of container vessel. *Transportation Research Part D: Transport and Environment*, *84*, 102389.

Valanto, P., & Hong, Y. (2015). Experimental investigation on ship wave added resistance in regular dead, oblique, beam, and following waves. *Proceedings of the 25th International Society of Offshore and Polar Engineers*.

Wang, H., Mao, W., & Eriksson, L. (2017). Benchmark study on different weather routing optimization algorithms.

Wang, H., Lang, X., Mao, W., Zhang, D., & Storhaug, G. (2020). Effectiveness of 2D optimization algorithms considering voluntary speed reduction under uncertain metocean conditions. *Ocean Engineering*, *200*, 107063.

Wang, H., Mao, W., & Eriksson, L. (2019). A Three-Dimensional Dijkstra's algorithm for multi-objective ship voyage optimization. *Ocean Engineering*, *186*, 106131.

Wang, X., & Teo, C. (2013). Integrated hedging and network planning for container shipping's bunker fuel management. *Maritime Economics & Logistics*, *15*, 172–196.

Woud, H. K., & Stapersma, D. (2002). *Design of propulsion and electric power generation systems*. MarEST, Institute of Marine Engineering, Science; Technology.

Zhang, C., Zhang, D., Zhang, M., & Mao, W. (2019). Data-driven ship energy efficiency analysis and optimization model for route planning in ice-covered Arctic waters. *Ocean Engineering*, *186*, 106071.